



**US Army Corps  
of Engineers**

Construction Engineering  
Research Laboratories

USACERL Technical Report 98/14  
December 1997

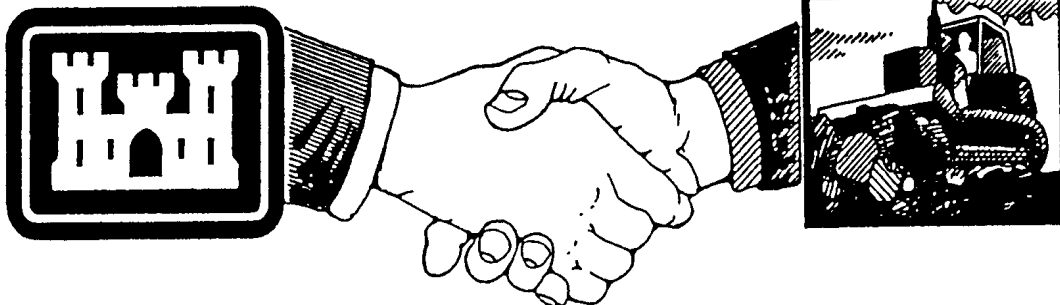
# CONSTRUCTION PRODUCTIVITY ADVANCEMENT RESEARCH (CPAR) PROGRAM

Development of Recycled Polymer Blends  
for Thermal Spray Applications

by

J. Brogan, C.C. Berndt, S. Sampath, H. Herman, and S.A. Drozd

Approved for public release; distribution is unlimited.



**A Corps/Industry Partnership To Advance  
Construction Productivity and Reduce Costs**

## SF 298

A proposed rule to implement Section 183(e) of the Clean Air Act amendments (1990) will further restrict the volatile organic compound (VOC) content of rust-preventing coatings. Thermal spray polymers represent one option for protecting steel structures while complying with the new VOC restrictions. Thermal spray technology can apply polymer coatings to many different substrate materials at various thicknesses and under wide range of ambient conditions. Potential benefits of thermal spray polymers could be extended by blending post-consumer commingled polymers (PCCP) into coating feedstock materials; thermal spray polymers have the potential both to lower material costs and reduce the volume of the solid waste stream. This research investigated and demonstrated high-molecular weight and commingled/postconsumer recycled polymer blends as low-VOC thermal spray coatings.

It is concluded that the incorporation of PCCP into virgin thermal spray polymer is associated with some loss of coating performance. Also, cost savings resulting from blending 25 percent PCCP with 75 percent virgin polymer are insignificant compared to the total cost of a recoating job using other VOCcompliant systems. Therefore, the blends investigated here probably will not have significant commercial usefulness, and they are not recommended for corrosion protection of steel structures.

## Foreword

This study was conducted for Headquarters, U.S. Army Corps of Engineers under Construction Productivity Advancement Research (CPAR) Work Unit 6L2, “Development of Innovative Hi-Molecular Weight and Commingled/Recycled Polymer Blends for Thermal Spray Applications.” The technical monitors were D. Casapula, CECW-EE, and A. Chandry, CECW-OM.

This CPAR work unit was coordinated through the Materials Science and Technology Division (FL-M) of the Facilities Technology Laboratory (FL), U.S. Army Construction Engineering Research Laboratories (USACERL). The work was conducted through a CPAR Cooperative Research and Development Agreement (CRDA) between USACERL and The State University of New York (SUNY) at Stony Brook. The USACERL Principal Investigators were Richard G. Lampo and Susan A. Drozdz, CECER-FL-M. The SUNY Principal Investigator was Dr. Christopher C. Berndt. Dr. Ilker R. Adiguzel is Acting Chief, CECER-FL-M, and Donald F. Fournier is Acting Operations Chief, CECER-FL. The USACERL technical editor was Gordon L. Cohen, Technical Information Team.

COL James A. Walter is the Commander of USACERL and Dr. Michael J. O'Connor is the Director.

# Contents

<b>SF 298</b> .....	1
<b>Foreword</b> .....	2
<b>List of Figures and Tables</b> .....	4
<b>1 Introduction</b> .....	7
Background .....	7
Objective .....	8
Approach .....	9
<b>2 Technology and Experimental Techniques</b> .....	10
Thermal Spray Processing of Polymers .....	10
Thermal Spray Torches .....	10
Polymer Powder Analysis .....	11
Testing and Analysis Technologies .....	12
<b>3 Experimental Results</b> .....	19
Flame Spray Processing of Virgin Polymers .....	19
Flame Spray Processing of Recycled Polymer Blends .....	26
Mechanical Properties of Polymer Materials and Blends .....	29
EMAA Adhesion to Steel .....	32
<b>4 Field Application</b> .....	62
<b>5 Cost Considerations</b> .....	64
<b>6 Conclusions, Recommendations, and Commercialization</b> .....	65
Conclusions .....	65
Recommendations .....	66
Commercialization and Technology Transfer .....	66
<b>References</b> .....	69
<b>Appendix: Equipment and Instrumentation Vendors</b> .....	71
<b>Distribution</b>	

## List of Figures and Tables

### Figures

1	Schematic of combustion spray torch . . . . .	16
2	The effect of gas mixture upon (a) flame temperature and (b) flame length . . . . .	17
3	Construction of peel test jig . . . . .	18
4	Peeled polymer coating from abrasive-blasted substrate . . . . .	18
5	Ethylene methacrylic acid copolymer powder . . . . .	36
6	Cross-section of coating with low splat elongation ratios . . . . .	38
7	Cross-section of coating with high splat elongation ratios . . . . .	39
8	Distribution of elongation ratios for the microstructural extremes . . . . .	39
9	Relationship between elongation ratio and surface roughness . . . . .	40
10	Relationship between surface roughness and deposit temperature . . . . .	40
11	Relationship between splat elongation ratio and deposit temperature . . . . .	41
12	Morphology of post-consumer commingled plastic after grinding . . . . .	41
13	Cross-section of post-consumer commingled polymer coating . . . . .	42
14	Surface of as-sprayed PCCP coatings from dry compounded recycled plastic . . . . .	43

15	Surfaces of weathered polymer coatings . . . . .	44
16	Cracking mechanisms for recycled post-consumer commingled polymer blends: (a) interfacial debonding, (b) crack intersection, (c) inter-particle cracking and (d) radial cracking . . . . .	45
17	Pseudo crack density of exposed coatings . . . . .	45
18	Average crack length for exposed coatings . . . . .	46
19	Tensile adhesion strengths for PCCP coating blends . . . . .	46
20	Stress-strain response of PF111 when pigmented, clear, and quenched . . . . .	48
21	Selected mechanical properties for PF111: a) modulus, b) tensile, c) elongation to break, and d) toughness . . . . .	49
22	Stress-strain response for PF113 when pigmented, clear, and quenched . . . . .	50
23	Selected mechanical properties for PF113: (a) modulus, (b) tensile, (c) elongation to break, and (d) toughness . . . . .	51
24	Stress-strain response for PCCP blends; volume percent PCCP noted on plot . . . . .	52
25	Mechanical properties of PCCP blends: (a) yield strength, (b) tensile strength, (c) secant modulus, and (d) elongation to break . . . . .	53
26	Summary of peel strength obtained for various steel surfaces . . . . .	55
27	Load-displacement plot for PF111 on polished steel . . . . .	55
28	Polymer fracture surface from polished steel depicting bands at (a) low and (b) higher magnification . . . . .	56
29	Load-displacement plot for PF111 on polished steel . . . . .	57
30	Peeling fracture surfaces from abrasive-blasted steel (a) PF111 and (b) PF113 . . . . .	58

31	EMAA peeled from abrasive-blasted steel . . . . .	59
32	(a) Load displacement plot for as-received steel surface and (b) SEM micrograph of polymer coating surface . . . . .	60
33	Proposed interfacial interactions between EMAA copolymer and steel oxide . . . . .	61
34	Field demonstration at the Triborough Bridge: (a) preheating the steel panel and (b) deposition of recycled polymer blend . . . . .	63

### Tables

1	Thermal-spray parameters for design of experiments study . . . . .	37
2	$2^{5-1}$ design for EMAA copolymer . . . . .	37
3	Statistically significant parameters* . . . . .	38
4	Bulk properties of individual polymer constituents . . . . .	42
5	Summary of spray-formed EMAA mechanical properties . . . . .	47
6	Mechanical properties of melt-compounded PCCP with EMAA copolymer . . . . .	52

# 1 Introduction

## Background

Protecting the infrastructure from the effects of corrosion is an increasing concern for the Army and the nation in general [1]. The average age of many bridges, locks, and dams exceeds 40 years, so maintenance is essential to ensure their reliability and safety of the populace. Choosing a method of corrosion protection is essentially a materials selection process, in which one chooses a protective coating system and perhaps a cathodic protection scheme [2, 3, 4]. Factors that influence this choice include the forms of corrosion encountered, exposure conditions (which range from mild atmospheric to industrial or marine), the type of structure and its condition, geographic location, and budget.

A proposed rule to implement Section 183(e) of the Clean Air Act, as amended in 1990, will limit the volatile organic compound (VOC) content of rust-preventing coatings to 400 grams per liter (61 FR 3279–32746; 40 CFR 59). When this rule takes effect on 1 January 1998, VOC content will be a major factor in the selection of protective coatings, and some coating systems used today (i.e., high-VOC alkyds, urethanes, and epoxies) will be prohibited [7]. Alternative technologies and non-solvent based coating materials and application technologies are currently being researched. Thermal sprayed thermoplastic is one viable option for meeting the construction industry's needs while complying with environmental restrictions; it is a 100 percent solids process that releases minimal VOCs [8]. Relatively thin (0.127 mm [0.005 in.]) to thick (6.35 mm [0.250 in.]) polymer coatings can be applied onto a wide variety of substrate materials to produce protective barrier coatings [5, 6]. Thermoplastic spraying has potential as an alternative to paint and other solvent-borne formulations.

In 1994 the U.S. Army Construction Engineering Research Laboratories (USACERL) published a technical report on an evaluation of flame-sprayed polymer coatings for civil works navigation structures [9]. The coatings were not recommended for use at that time because of their relatively poor performance in laboratory and field tests. The coatings were tested in immersion in fresh and salt waters in addition to atmospheric exposure. An ethylene-acrylic acid copolymer provided the best performance in all exposures, but its expected service life of 5

years in immersion service compares poorly to the 15 to 20 years for currently used vinyl systems. Adequate performance and an 8 to 10 year service life was estimated for atmospheric weathering — much shorter than the 20 to 30 years of protection provided by standard Army Corps of Engineers systems.

Despite its unremarkable performance in these tests, thermal spraying of polymers offers a number of compelling potential benefits for the U.S. construction industry. However, successful applications will require the definition of structural types, substrates, and environmental conditions for which thermal-sprayed polymers can be used. Polymer spraying is a one-coat process; the coating acts as both primer and topcoat. The coating requires no additional cure times (unlike the traditional multicoat painting processes) [6]. Thermal spraying is adaptable to structures of any size. Unlike electrostatic powder coatings, this process can coat nonconductive components (e.g., concrete, plastic, fiberglass) and can be used on heat-sensitive materials (e.g., wood and wood products). Thermoplastic materials can always be remelted and will fuse with new material in the molten state, so it is possible that these coatings could be repaired by simply remelting or applying additional material to the damaged area. In addition, a report on thermal spray powder coatings [10] shows that because these coatings do not rely on solvent evaporation for film deposition, polymers such as ethylene methacrylic acid copolymer (EMAA) can be applied in high humidity as well as in temperatures below freezing — conditions under which traditional paint systems often may not successfully be applied.

The potential benefits of polymer thermal spraying could be extended further by the incorporation of post-consumer (recycled) polymers into the coating feedstock. However, the use of commingled recycled polymer materials into thermal spray polymer coatings has not been reported in the literature. Commingled polymer, also referred to as "curbside tailings," is a mixture of many types of thermoplastics, and often contains paper, aluminum, and glass particulate wastes. This particular blend of plastics is the remaining yield after high-value polymer components such as polyethylene terephthalate (PET) and high-density polyethylene (HDPE) are separated out. It is therefore of considerable interest to determine the viability of using recycled and post-consumer commingled polymer in the form of coatings to reduce cost as well as reduce the amount of waste disposal.

## Objective

The objective of this program was to develop and demonstrate innovative high-molecular weight and commingled/post-consumer recycled polymer blends as low-VOC coatings for thermal spray application.

## Approach

Thermal sprayed polymeric coatings are generally applied by melting polymer powder in a combustion flame or plasma stream. The material carried by the heated gas is deposited as "splats" (or droplets of molten plastic) on the substrate surface, where it fuses and consolidates into a coating film. Thermal spray equipment, designed exclusively for polyethylene-based polymers (as marketed by Plastic Flamecoat Systems, Big Spring, TX), allows simultaneous thermoplastic deposition and fusion. Ethylene methacrylic acid copolymer (EMAA) is the most commonly used polymer in the field, but little structure-property data are reported in the open literature. In this study, commercially available equipment and EMAA copolymer powder were used for laboratory and field applications.

A design of experiments approach was used to determine how the thermoplastic microstructure is affected by variations in process parameters such as substrate and coating temperature, flame setting, and standoff distance. Mechanical properties were then assessed to determine optimum processing conditions.

The research objective included the characterization of coatings produced from post-consumer commingled polymer (PCCP). The objective is complicated by the fact that incompatible polymers in the commingled mix would melt and coalesce during thermal spraying. To address this problem, PCCP was blended in various percentages with virgin EMAA copolymer for improved performance. The properties of commingled polymer coatings were compared to virgin EMAA coatings to assess whether the use of these waste materials is accompanied by a degradation in mechanical properties.

Commingled polymer particulates experience a variety of thermal histories depending upon their individual thermal diffusivity, particle size, molecular weight, residence time, and position within the flame. These factors in turn influence the degree of polymer flattening as well as the rate of cooling and solidification. Microstructural features (splat elongation ratio), polymer structure and chemistry (oxidation, crystallinity, molecular weight), adhesion, and mechanical properties were analyzed in relation to selected processing parameters. Specifically, analyses were conducted to determine such structure-property relationships for EMAA copolymer, to understand the mechanisms affecting adhesion to steel surfaces, and to characterize PCCP-based coatings.

## 2 Technology and Experimental Techniques

### Thermal Spray Processing of Polymers

In the thermal spray polymer coating application process, the polymer powder is axially fed into the combustion zone via a carrier gas. The polymer particles are propelled through the flame, where they melt into droplets and are transported to a preheated substrate. As the molten particles hit the substrate, the molten particles deform and solidify, creating an interlaced network of “splats.” Porosity within the coating depends upon the coating temperature, nature of the substrate surface, and the polymer melt-viscosity. The thickness of the coating is governed by droplet velocity, rate of spray gun movement, and number of passes across the substrate.

Polymer powders are specified by their chemistry, morphology, molecular weight distribution and associated melt-flow index, and particle size distribution. Spray parameters must be selected to accommodate each particular polymer formulation. A larger thermal input is required to melt larger particles and higher molecular weight organic molecules. A large particle size distribution or molecular weight distribution may facilitate the formation of numerous heterogeneities within the coating microstructure, creating voids, a range of splat aspect ratios, and degraded material. A “processing window” exists for each polymer, where poor particle coalescence defines the lower limit and pyrolysis defines the upper limit. It is also important to note that, even within the processing window, the polymer may also cross-link, undergo chain scission, or oxidize.

### Thermal Spray Torches

#### *Plastic Flamecoat 200 Torch*

The PFS 200 gun (marketed by Plastic Flamecoat Systems [PFS], Big Spring, TX) is the prototype torch initially used in the course of this research [14]. This particular torch uses compressed air as both the oxidant for combustion and as the carrier gas to propel the powder through the flame. Recommended specifications include 283 l/min (10 cfm) of air at 414 kPa (60 psi) as well as 5–15 pounds of

propane pressure. Powder is conveyed via compressed from a gravity-fed hopper. Flame air, propane flow rate, and powder flow rate can independently be controlled. The larger torch PF400 has a 4-in. (10 cm) diameter nozzle in comparison to the standard two-inch design.

#### ***Plastic Flamecoat Powder Pistol 124***

The Powder Pistol 124, the company's second-generation combustion-spray gun, is connected to a fluidized bed powder feeder (Figure 1).<sup>\*</sup> Propane and compressed air are used as the fuel and oxidant for the combustion process. The air supply pressure ranges from 621-827 kPa (90-120 psi) and generally is consumed at 198 l/min (7 cfm). The air supply should be free of oil and moisture. The compressed air supply provides air for the propane/air mixture, provides air for powder transport through the flame, and provides air to fluidize the powder. The powder feeder can hold a maximum of 10 lb (4.5 kg) EMAA powder. In addition, the maximum application rate is approximately 8 lb/hr. The recommended propane supply pressure ranges from 90-117 kPa (13-17 psi) and generally is consumed at 1.5 lb/hr (0.68 kg/h). The flame air, fluidized bed air, powder feed rate, and propane flow rate can be independently controlled. It should be noted that a retrofit is available, increasing polymer application rates to 12.5 lb/h (5.7 kg/h).

### **Polymer Powder Analysis**

EMAA powder was received from Plastic Flamecoat Systems. Pigments are incorporated using dry compounding or melt compounding procedures. Proprietary additives, including UV-light stabilizers, antioxidants, and flow enhancers are also blended to optimize coating properties and ease of processing. The base-polymer is cryogenically ground to -70 mesh (< 212 micrometers), resulting in a particle morphology is angular and faceted. The particle becomes more spherical in shape during the melt-compounding operation because the particle is heated above its crystalline melting point. Consequently, it is more difficult to fluidize or feed the unpigmented powder due to its angular morphology.

Two EMAA powders were used in this research: PF111 and PF113. Powder size distributions were obtained using Micro Trac Powder Analysis. The average size, assuming a spherical shape factor was 140 micrometers with a standard deviation of 70 micrometers. Ninety percent of the powder was also less than 220 micrometers. These powders were chosen on the basis of availability and the

---

<sup>\*</sup> Figures and tables are presented at the end of the chapter in which they are first referenced.

discernible difference in melt-flow characteristics. As previously noted, EMAA copolymer has the best balance of performance properties (i.e., adhesion and permeability).

## Testing and Analysis Technologies

### *Flame Temperature*

Flame temperatures were measured with a thermocouple at 5 cm (approximately 2 in.) intervals from the nozzle. The highest flame temperature was approximately 1300 °C (2370 °F). Temperatures and flame lengths were dependent upon the flame stoichiometry. Figure 2 summarizes the effects of gas mixture upon temperature and flame length. The higher the air-to-fuel ratio, the higher the flame temperature at distances close to the nozzle (5-10 cm [2-4 in.]). Peak temperatures for fuel-rich flames were observed further downstream as reflected in the data at 45 cm (approximately 18 in.). Fuel-rich flames were also much longer in length, approximately 50 cm (20 in.) compared to approximately 12 cm (5 in.) for a high air-to-fuel ratio.

### *Melt Flow Indexer*

The melt flow indexer is an industrial device used to assess the molecular weight of polyethylene. A melt flow indexer, also referred to as an extrusion plastometer (Tinius Olsen, Willow Grove, PA), was used at PFS. To use this technology, approximately 4–5 grams of polymer is placed into the loading cell. The material is heated to 190 °C (374 °F) for 6 minutes. A 2.16 kg (4.75 lb) load is also applied during the melt, inducing a pressure of 3.0 bar (3032.148 g/cm<sup>2</sup>). The molten polymer is allowed to flow through an orifice for 1 minute, and the extruded plastic is then weighed. The melt flow index (MFI) is the output rate in g/10 minutes from a standard die of 2.1 mm diameter and 8.0 mm length. The MFI is an inverse measure of melt viscosity. Therefore, the higher the melt flow index, the lower the average molecular weight.

The PF111 powder has a melt-flow index of 32 g/10 min and a density of 0.934 g/cm<sup>3</sup>. In contrast, PF113 has a higher melt-flow index, 500 g/10 min and a lower density, 0.918 g/cm<sup>3</sup>.

### ***LaserStrobe™ Control Vision***

Particle velocities were measured using a LaserStrobe™ Control Vision System (Idaho Falls, ID). This system uses two nitrogen laser strobes (5 ns pulse width) with fiber optic cable, to transport and focus 337 nm light to the area of interest. The high speed electronic shutter (50 ns to 5  $\mu$ s) is synchronized with the laser flashes. The laser is also synchronized with the framing of the video sensor (5 ns at 337 nm) and is fired once for each captured video frame. The image of the moving particle is effectively frozen in space and—in double exposure—displaced in flight. Particle velocity is calculated from the laser synchronization time and particle displacement [15].

### ***Light Microscopy (LM)***

Material specimens were cut with a diamond saw, mounted in cross-section, and polished using a Buehler automated polishing machine. A two-light microscope (Unitron-Versamet, Plainview, NY) was used in reflection to observe coating microstructures. Lamellae (crystalline regions) were best visualized when using darkfield illumination. This was accomplished by setting the epi-diaphragm lever to “D,” adjusting the polarizer to 90 degrees, and removing both the analyzer and the interference prism from the light path.

Coatings were also sectioned using a microtome to obtain optically transmissive specimens. Polarized optics were used in transmission to detect spherulitic\* features. Anisotropy is present when black and white contrast is visualized. Polarized optics were obtained by setting the epi-diaphragm lever to “B,” setting the polarizer to 0° setting the analyzer to 90° and removing the interference prism from the image path.

### ***Scanning Electron Microscopy (SEM)***

Polymer powder, coating surfaces, and coating cross-sections were sputtered\*\* with gold and analyzed with an ISI-SX-30 scanning electron microscope. The accelerating voltage was 15 kV (unless otherwise stated in text). Secondary electron images were used to examine fracture surfaces, and back-scattered electron images were used to assess pigment agglomeration and other chemistry-dependent features.

---

\* spherulitic: crystals arranged in the general form of a sphere.

\*\* sputtering: a technique for depositing metal atoms on plastic or other substrate.

### ***Surface Profilometry***

The surface roughness, Ra, was measured using a Mitutoyo SurfTest III (Japan). This device uses a mechanical stylus to traverse the specimen surface and measure the average deviation of the surface from a centerline value. Various scanning speeds and cutoff values can be selected to examine the surface. General surface waviness can be assessed using a 6 mm/sec scan rate and a 2.5 cutoff value. Roughness within the surface undulations can be assessed using a 2 mm/sec scan rate in conjunction with a 0.08 cutoff value.

### ***Differential Thermal Analysis (DTA)***

Polymer powder and coatings were analyzed with a Stanton Redcroft STA 780. Approximately 10–20 mg of material was placed in a platinum crucible and heated from 25 to 600 °C (77 to 1112 °F) at a heating rate of 5 °C /min. The constant heating rate is applied to both the experimental sample and a reference sample. Because energy input remains constant, differences in temperature between the two samples are measured as a function of temperature or time as the sample is heated. The temperature peaks are related to enthalpic reactions due to both physical and chemical changes to the polymer structure.

### ***Thermogravimetric Analysis (TGA)***

Thermogravimetric analysis was conducted simultaneously with DTA on the Stanton Redcroft STA 780. This technique records the weight of a sample as a function of time or temperature. As previously discussed, the heating rate in this study was 5 °C/min. Data pertaining to polymer volatilization and decomposition were obtained.

### ***Differential Scanning Calorimetry (DSC)***

Differential scanning calorimetry was performed on a Dupont 2100 V4.OB unit. This technique is based on heating or cooling an experimental sample and a reference sample at a predetermined rate. Unlike DTA, the temperature of both the experimental sample and the reference sample is kept constant while the heat flux is measured. The heat flux is directly related to the enthalpy, so, heats of reaction can be quantified. Approximately 8–10 mg samples of polymer were heated from -30 °C to 150 °C at 10 °C per minute. DSC was used to determine the temperatures at which the polymer transitions from a hard, brittle material to an elastomer (glass transition temperature) and from an elastomer to a liquid (melt temperature).

### ***QUV Weathering Chamber***

The QUV accelerated weathering tester is a light- and water-exposure testing apparatus that simulates the damaging forces of ultraviolet (UV, from sunlight) and rain. Coatings were sprayed in triplicate onto 4 in. X 6 in. (approximately 10 X 15 cm) abrasive-blasted steel of 1/8 in. (3.2 mm) thickness and subjected to accelerated QUV weathering tests according to ASTM G 53-88. A carbide-tipped scribe was used to scrape an "X" on the coating surface. Samples were exposed to cyclic conditions of ultraviolet light, 280-315 nm (UV-B) at 60 °C (140 °F) and to condensation at 50 °C (122 °F) every 4 hours for a total of 1250 hours. Samples were rotated once a week to ensure uniform exposure. Ultraviolet lamps were rotated every 500 hours in accordance with manufacturers specifications.

### ***Tensile Testing***

Techniques were developed to produce freestanding polymer coatings. The first method involves painting a water-soluble debonding layer (Metco De-Bond, Westbury, NY) on the surface of a steel plate and allowing the layer to dry for 24 hours. Polymer powder was then sprayed directly onto this debonding layer; however, the propane flow rate was decreased during the first few passes to prevent vaporization of the debonding layer. The propane flow was then increased to the desired rate and coatings were deposited to the appropriate thickness. Once the polymer cooled, an exposed edge was immersed in water, allowing the coating to be easily removed from the substrate. Although freestanding polymer components can be prepared in this fashion, high application temperatures degrade the debonding agent, and this produces porosity in the polymer coating.

The second method of preparing free-forms entails spraying the molten polymer directly onto a Teflon<sup>TM</sup>-coated skillet. Since the fluoropolymer has such a low surface energy, the polymer coating does not adhere to the skillet surface allowing easy removal. This method has significant advantages over the water-soluble layer method and was thus used for all testing of polymer mechanical properties.

To minimize surface flaws that may arise from cutting, a die-stamp was used to produce reproducible ASTM D632 Type IV "dog-bone" specimens. The tensile test specimens were also polished to ensure uniform sample thickness. Tensile testing was conducted on a system manufactured by Applied Test Systems (ATS). A 1000 lb load cell measured the load to maintain a constant displacement rate. Data were collected at 80 Hz using a data acquisition package. Load and displacement values were converted to engineering stress and strain using a strain rate of 2 inches per minute (5 cm/min). The effects of pigment, melt-flow index, and cooling rate were

also assessed. A minimum of eight samples were tested for each condition to establish a standard deviation.

### ***Peel Adhesion Testing Rig***

In order to assess the polymer adhesion to steel, a 90 degree peel test rig was constructed according to ASTM D 3167 specifications. The geometry consists of two parallel plates held one in. apart by three studs (Figure 3). Two 1-in. diameter mandrels are set in needle roller bearings to allow the substrate to traverse as the load is applied. This construction permits the jig to align itself as well as allow the sample to climb during the experiment.

Steel substrates measuring 6 in. in length, 1 in. in width, and 1/8 in. thickness were used in this study. Self-adhering aluminum tape was initially fastened to one end of the steel substrate. A polymer coating of approximately 625 micrometers (25 mils) was then deposited over the tape/steel assembly. The extended tab was fastened to the grips of an ATS tensile testing machine and subsequently pulled 90 degrees from the steel substrate. This procedure allows the crack to propagate along the polymer/steel interface at the peel speed, specified as 152 mm/min (6 in./min). Figure 4 illustrates the crack direction as the plastic adhere is peeled from an abrasive-blasted steel substrate. The force required to propagate the crack was recorded on a digital acquisition board at a rate of 8 Hz.

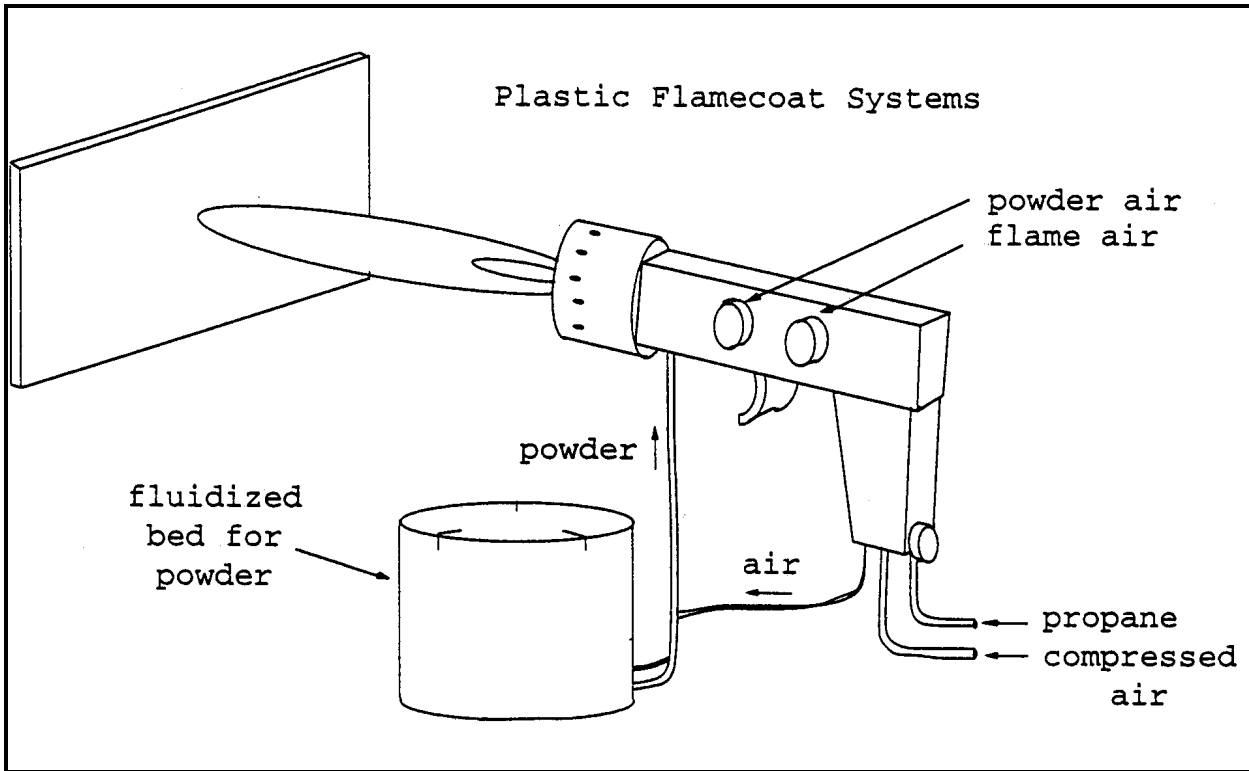


Figure 1. Schematic of combustion spray torch.

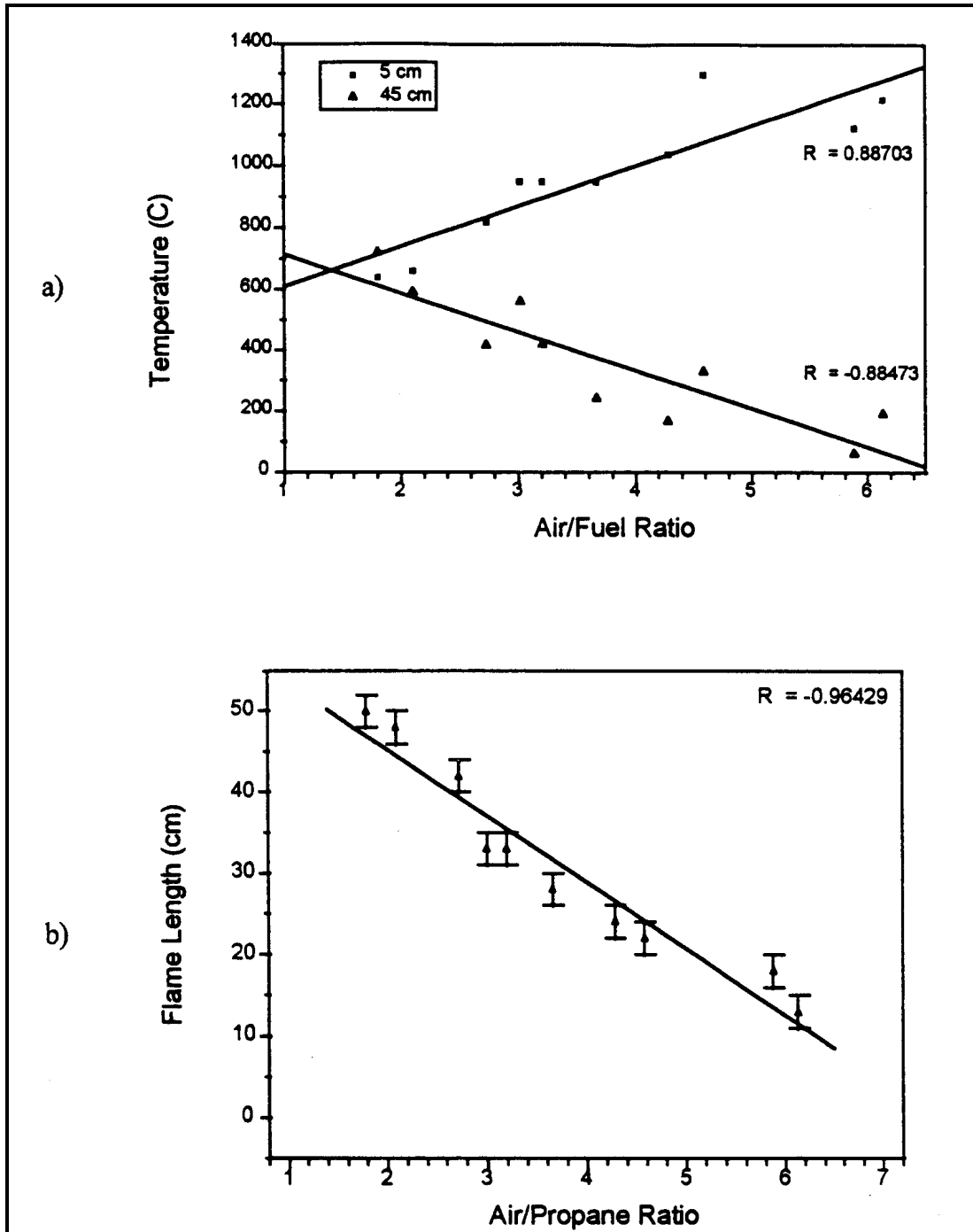


Figure 2. The effect of gas mixture upon (a) flame temperature and (b) flame length.

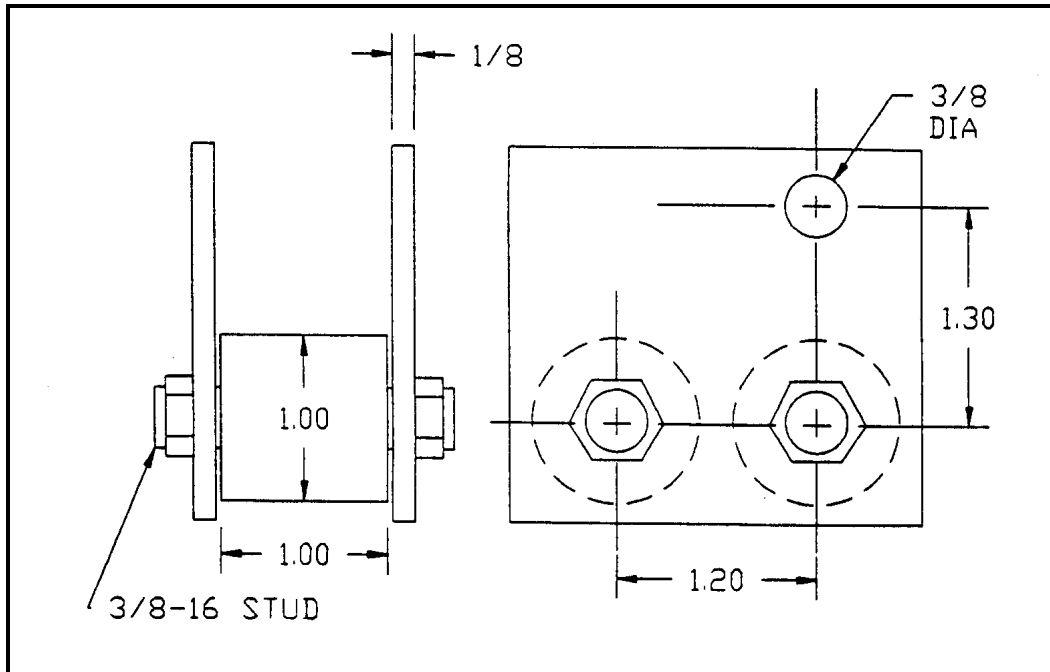


Figure 3. Construction of peel test jig.

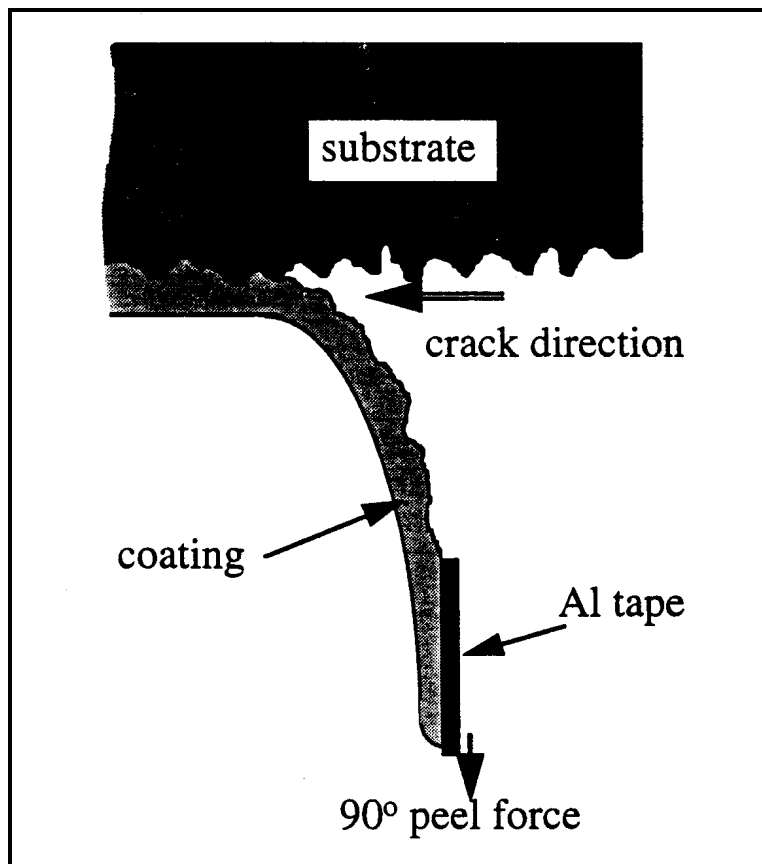


Figure 4. Peeled polymer coating from abrasive-blasted substrate.

### 3 Experimental Results

#### Flame Spray Processing of Virgin Polymers

A design of experiments approach was employed to study the coalescence of combustion-sprayed ethylene-methacrylic acid (EMAA) copolymer [16]. The EMAA was obtained from Plastic FlameCoat Systems as PF113W (Figure 5). This powder was dry compounded with TiO<sub>2</sub> pigment as well as with proprietary thermal and UV light stabilizers. PF113 has a melt index of 500 g/10 min, corresponding to the lowest average molecular weight copolymer in the EMAA series. This polymer was chosen on the basis of its sensitivity to temperature, which allowed precise processing/structure evaluations to be made.

Thermogravimetric analysis and differential thermal analysis were conducted simultaneously on the PF113 powder. The first endothermic peak began at 72 °C and ended at 96 °C, characteristic of the polymer melting point region. Weight loss initially occurred at 260 °C losing 5 percent of the weight between 260 and 390 °C. This may signify stabilizer decomposition since an endothermic peak was observed on the DTA trace at 260 °C. At 390 °C an endothermic peak on the DTA trace was observed, representing polymer vaporization. This transition was directly reflected on the TGA spectrum because 75 percent weight loss occurred from 390 to 470 °C. The thermal analysis therefore suggests that PF113 can be processed between the temperatures of 94–260 °C (201–500 °F) without weight loss. The maximum processing temperature before polymer vaporization is 390 °C (734 °F).

Since a large processing window was verified using DTA/TGA, it was hypothesized that a range of splat morphologies is likely to exist during spray processing. A 2<sup>5-1</sup> factorial design matrix was chosen for EMAA copolymer to determine the processing factors responsible for changes in the coating microstructure. Using a two-level design, process parameters were varied from a low value (-) to a high value (+), and the effect upon a particular response (Y) is measured [17]. The “effect” is calculated by subtracting the average response using the low parameter from the average response using the high parameter setting, i.e.,

$$\text{Effect} = \frac{\sum Y_+}{n_+} - \frac{\sum Y_-}{n_-} \quad (1)$$

Interactions between parameters can also be detected and quantified [17]. Influential process parameters can, therefore, be identified on the basis of the induced effect. The underlying objective of empirical modeling is to relate  $N$  coded process parameters  $X_i$  ( $i=1\dots N$ ; here:  $N=5$ ) to  $M$  responses  $Y_j$  ( $j=1\dots M$ ; here:  $M=3$ ) of the form

$$Y_i = \beta_0 + \beta_1 X_1 + \beta_2 X_2 + \beta_{12} X_1 X_2 + \beta_3 X_3 + \beta_{13} X_1 X_3 + \beta_{23} X_2 X_3 \dots + \beta_{iN} X_i X_N \quad (2)$$

where the beta coefficients are regression coefficients calculated from the measured effect [14], i.e.:

$$\beta = \frac{\text{Effect}}{2} \quad (3)$$

The “ $X_i$ ” terms in the polynomial equation are coded process parameters representing the selected parameter value multiplied by an empirical factor calculated from the chosen high and low values (+ and -, respectively):

$$X_{\text{coded}} = \frac{X - [(+) + (-)]}{[(+) - (-)]} \quad (4)$$

This allows prediction of a particular response on the basis of the selected process parameters.

The present model entails setting five parameters (powder feed rate, standoff distance, substrate preheat temperature, propane flow rate, and compressed air flow rate), at two levels (+ and -), measuring three responses (surface roughness, coating temperature, and splat elongation ratio), and calculating the effects due to each parameter and parameter interaction. A design of experiments software package, Design-Ease (Statease Inc., Minneapolis, MN), was used to generate the half-factorial matrix, calculate the single parameter and interaction effects, and provide the analysis of variance (ANOVA). Three additional sets of parameters using mean high / low values were also used to account for nonlinearity as well as to determine the repeatability of the deposition process, giving a total of 19 experiments. A number of fixed and variable parameters were selected on the basis of thermal spray experience (Table 1). A six-axis articulated robot was used to ensure that the traverse speed, standoff-distance and spray step distance remained constant during spraying. Although a traverse speed of 25 cm/sec is faster than one

would normally use in practice, it was used to ensure minimal flame contact with the coating.

Upon completion of each experiment in the matrix, a remote infrared pyrometer measured the surface temperature of the sprayed deposit (noted as response 1). The surface roughness,  $R_a$ , was measured as previously described in section 3.7 (noted as response 2). The microstructure was visualized with light microscopy. Buehler image analysis software (Buehler, Lake Bluff, OH) was used to trace the individual polymer lamellae, and the results were then digitized for subsequent measurements. Thirty splats per sample were analyzed to determine the average elongation ratio of the splat (noted as response 3).

The components of the  $2^{5-1}$  factorial matrix as well as the measured responses for each set of experimental conditions are listed in Table 2. Using a traverse speed of 25 cm/sec, coating surface temperatures ranged from 60–180 °C, surface roughness ranged from 50 micrometers to 3 micrometers, and splat elongation ratio ranged from 1.59 to 7.33. Table 3 summarizes the parameters and parameter combinations inducing the greatest effects on the responses. The powder feed rate had the greatest impact on coating microstructure and macrostructure (splat morphology and surface roughness, respectively). Substrate preheating had the greatest effect on the coating surface temperature.

### **Coating Temperature**

The temperature of the deposited thermoplastic coating depends upon the substrate preheat temperature,  $X_3$ , the propane flow rate,  $X_4$ , and the powder feed rate,  $X_2$ . Standoff distance,  $X_2$ , and the interaction between standoff distance with compressed air,  $X_{25}$ , are also included in the model. An increase of substrate temperature from ambient to 87 °C increased the coating temperature from 85 to 151 °C (effect = 66 °C) when averaged over all parameter combinations in the matrix. Increasing the propane flow rate from its low flow setting to the high flow setting increases the coating temperature from 106 to 131 °C (effect = 25 °C). Since the length of the flame increases with the propane flow rate, higher particle temperatures result due to greater residence times within the flame. The average coating temperature increased from 107 to 130 °C (effect = 23 °C) when the powder injection rate increased from 70 g/min to 140 g/min. The polynomial equation which empirically predicts the coating temperature (in °C) to within 5 percent is:

$$Y_{\text{temperature}} = 118.3 + 11.5X_{1\text{coded}} + 5.8X_{2\text{coded}} + 33.1X_{3\text{coded}} + 12.5X_{4\text{coded}} - 6.1X_{2\text{coded}}X_{5\text{coded}} \quad (5)$$

where the coded  $X_i$  terms are as shown below and are applicable to each of the empirical equations representing coating temperature, surface roughness, and splat elongation ratio.

$$X_{1\text{coded}} = \frac{X_1 - 105}{35} (\text{g/min}) \quad (6)$$

$$X_{2\text{coded}} = \frac{X_2 - 37.5}{12.5} (\text{cm}) \quad (7)$$

$$X_{3\text{coded}} = \frac{X_3 - 54}{33} (^\circ\text{C}) \quad (8)$$

$$X_{4\text{coded}} = \frac{X_4 - 10.9}{4.3} (\text{l/min}) \quad (9)$$

$$X_{5\text{coded}} = \frac{X_5 - 160}{40} (\text{l/min}) \quad (10)$$

The accuracy of this equation was assessed by using the process parameters from the design of experiments study (Table 2) and comparing the measured response to the predicted response. The 5 percent error represents the average residual from the experimental matrix.

### **Surface Roughness**

The roughness of EMAA coatings depends upon the powder feed rate  $X_1$ , substrate temperature  $X_3$ , substrate temperature/propane flow rate interaction  $X_{34}$  and powder feed rate/standoff distance interaction  $X_{12}$ . The propane flow rate  $X_4$  was also included in the model for increased accuracy. An  $\ln(Y_2)$  transformation was used to model the surface roughness due to the large variation in roughness values. The surface roughness decreased from 32 micrometers to 12 micrometers (effect = 20 micrometers) when the powder feed rate was increased from 70 g/min to 140 g/min. The surface roughness also decreased from 27 micrometers to 16 micrometers (effect = 11 micrometers) as the substrate temperature was increased from ambient to 87 °C.

Since both parameters are involved in significant interaction effects, it is essential to include such interactions in the empirical model. The surface roughness remained constant at low propane flow rates, even when the substrate temperature increased, but, the roughness decreased with increasing substrate temperatures at the high propane flow rate (effect = 9 micrometers). The second noteworthy interaction involves standoff distance and powder feed rate. The surface roughness decreased with increasing powder feed rate at both 25 and 50 cm. At lower feed rates, the roughness is lower for shorter standoff distances, but at higher powder feed rates, the roughness is lower at longer standoff distances (effect = 7 micrometers). The empirical equation used to estimate coating surface roughness (in terms of Ra in micrometers) is as follows:

$$1nY_{\text{roughness}} = 2.81 - 0.49X_{1\text{coded}} - 0.23X_{1\text{coded}}X_{2\text{coded}} - 0.31X_{3\text{coded}} - 0.21X_{4\text{coded}} - 0.22X_{3\text{coded}}X_{4\text{coded}} \quad (11)$$

Upon analysis of the residuals, Equation 11 was found to be accurate to within 10 percent of the measured surface roughnesses.

#### ***Microstructure: Splat Elongation Ratio***

The splat elongation ratio depends on powder feed rate  $X_1$ , standoff distance  $X_2$ , powder feed rate interacting with standoff distance  $X_{12}$ , and substrate preheat temperature  $X_3$ . A number of secondary effects  $X_{15}$ ,  $X_{25}$ ,  $X_{34}$ , and  $X_{45}$ —are also included. The largest effect was observed when the powder feed rate was increased to 140 g/min and thus increased the average elongation ratio from 3.3 to 4.8 (effect = 1.5). The average elongation ratio increased from 3.4 to 4.6 (effect = 1.2) when the standoff distance is increased from 25 cm to 50 cm. The elongation ratio also increases from 3.6 to 4.4 (effect = 0.8) when the substrate is preheated to 87 °C. The powder feed rate was also found to interact with standoff distance. The splat elongation ratio does not change with standoff distance at the low powder feed rate of 70 g/min. However, at the higher feed rate of 140 g/min, the average elongation ratio increased by approximately 2.2 when the standoff distance increased from 25 cm to 50 cm. The empirical equation used to estimate the splat elongation ratio (in nondimensional units) from knowledge of the chosen process parameters is:

$$Y_{\text{E.R.}} = 3.99 + 0.75X_{1\text{coded}} + 0.59X_{2\text{coded}} + 0.51X_{1\text{coded}}X_{2\text{coded}} + 0.58X_{1\text{coded}}X_{3\text{coded}} - 0.37X_{2\text{coded}}X_{3\text{coded}} + 0.41X_{3\text{coded}} + 0.34X_{3\text{coded}}X_{4\text{coded}} + 0.35X_{4\text{coded}}X_{5\text{coded}} \quad (12)$$

Again, as for the surface roughness equation (Equation 11), using the parameters from the experimental matrix and comparing the residuals, Equation 12 was found to be accurate to within 10 percent of the measured elongation ratio.

Differences in the melting and/or deformation behavior of EMAA copolymer can be discerned by examining the microstructures in cross-section. Figure 6 illustrates poor coating coalescence due to insufficient polymer melt-flow, as evident by spherical splats (line 7, Table 2). The degree of melting and coalescence in Figure 7 (line 16, Table 2) is higher, as evident by thin lamellae and a deformed impact geometry. The impinging molten polymer will flow around the underlying topography, thereby, increasing the density of splats.

The elongation ratio distributions for the poorly coalesced coating and highly coalesced coating are shown in Figure 8. The average elongation ratio for the microstructure in Figure 6 was 1.6 with a standard deviation of 0.4. Ninety percent of the coating contains particles with elongation ratios less than 2. In contrast, the average elongation ratio for the coating in Figure 7 was 7.3 with a standard deviation of 3.6. This coating, which corresponds to the lowest of measured surface roughness values, reveals that less than 2 percent of the deposit contains particles with elongation ratios lower than 2. It is common for poorly melted particles to exist in the coating because particles do not all follow the same trajectory through the flame, but this analysis quantifies the microstructural variation in thermal sprayed EMAA coatings.

### ***Response Correlations***

A general trend was observed between the average elongation ratio and surface roughness for each specimen in the matrix. Figure 9 illustrates that a greater surface roughness correlates to lower splat elongation ratios (and, thus, poor coalescence). From the design of experiments study, two factors seem responsible for the poor melt flow characteristics. One factor is the low thermal input to the polymer due to its short residence time within the flame. This produces insufficient particle melting and results in low elongation ratios. On the coating surface, low splat elongation ratios correspond to an agglomeration of fused polymer spheres. Areas of protruding polymer particulates yield a higher surface roughness, which defines a poorly coalesced coating. The second possible factor relates to the rate of polymer injection into the combustion zone. A low powder feed rate correlates to a lower amount deposited polymer per unit area. Less molten material can conform to the underlying topography. Discontinuous surface coverage will result in a higher surface roughness unless a slower traverse speed is used during application.

The temperature dependence upon surface roughness is shown in Figure 10. A high surface roughness was measured for coating temperatures lower than 80 °C. The surface roughness decreased by a factor of approximately 2 at temperatures greater than 90 °C. This temperature threshold between high to low surface roughness

correlates with the melting point of the copolymer. Data obtained from differential scanning calorimetry reveals that the primary endothermic melting point begins at 78 °C and peaks at 96 °C. However, the elongation ratio measurements (Figure 11) were not as sensitive to temperature as the surface roughness measurements. The elongation ratio only correlated to the coating temperature at the extreme temperature limits. The temperature region of 95-140 °C may be sufficient to reduce the surface roughness, but temperatures within this range are not sufficiently high to elongate the polymer splats. At 180 °C a noticeable increase in splat elongation ratio occurred. It also should be noted that the splat elongation ratio is a function of the original diameter of the polymer particulate. Larger polymer particles will remain more spherical in shape than smaller particles. Less energy is required to melt the fine particles, so smaller particles are more susceptible to deformation at the site of impact than the larger polymer particulates. Examining the correlations between the responses, a well-coalesced EMAA coating will result from an application temperature greater than 125 °C, and will exhibit a surface roughness less than 15 micrometers and a splat elongation ratio of at least 4.5.

### ***Particle Velocities***

A LaserStrobe™ Control Vision system was used to determine whether particle velocities were dependent upon the process parameters. The experimental technique was the same as previously described. Particle velocities (50 particles per data point) were measured at several standoff distances for both a high flame setting (high propane, high compressed air) and for a low flame setting (low propane, low compressed air). At a distance of 25 cm from the PF200 nozzle, average particle velocities are 14 m/sec and 10 m/sec for the high and low gas settings, respectively. The standard deviation was 5 m/sec, indicating that increasing gas flow rates do not appreciably affect the particle velocity. In addition, particle velocities at 50 cm from the nozzle are only slightly lower than at 25 cm, irrespective of gas settings. Variances in surface roughness and elongation ratio did not arise from differences in particle velocities since the velocities were found to be independent of the gas flow rates and standoff distance. The particle residence time varies from 3 ms for a 5 cm length flame to 20 ms for a 25 cm length flame. The flame stoichiometry did not appreciably affect the fusion of the polymer particulates.

### ***Discussion of EMAA Thermal Spray Tests***

The microstructure of a thermal sprayed polymer deposit is process-controlled. The substrate preheat temperature showed the largest effect on coating temperature. An empirical equation was developed to estimate coating temperature to within a 5 percent margin of error. The powder injection rate showed the largest effect on

coating surface roughness and the splat elongation ratio. Polynomial equations were experimentally determined for surface roughness and splat elongation ratio, and were accurate to within 10 percent.

Center-line particle velocities did not change with the gas flow rates or standoff distances used in this study (approximately 15 m/sec ), but differences in splat elongation ratio were observed. The particle residence time varied from 3 ms for a 5 cm length flame to 13 ms for a 20 cm length flame. The flame stoichiometry did not appreciably affect the fusion of the polymer particulates, so, for a fixed traverse speed, the particle residence time within the flame as well as the number of particles arriving at the substrate surface determines the extent of EMAA coating coalescence.

Based upon the correlations between the responses, a well-coalesced EMAA coating (melt flow index of 500 g/10 min) will have a temperature greater than 125 °C (257 °F), a surface roughness less than 15 micrometers, and a splat elongation ratio of at least 4.5. The coating temperature, surface roughness and microstructure can be estimated on the basis of the selected process parameters.

## Flame Spray Processing of Recycled Polymer Blends

### *Processing*

Post-consumer commingled polymer (PCCP) was received from Obex, Inc. (Stamford, CT) in the form of 3/8" flake. PCCP consists principally of different polyethylene densities and molecular weights, plus smaller concentrations of polypropylene, polystyrene, polyvinylchloride and polyethylene terephthalate. The polymer chips were washed to remove food debris and residue. Aluminum, glass, cardboard, and paper were extracted from the polymer blend. A cryogenic milling machine using liquid nitrogen coolant was employed to lower the temperature of the polymer to facilitate comminution\*. The ground polymer was sieved to -50 mesh, corresponding to an average particle size of 177 micrometers (Figure 12).

A combustion torch marketed by Plastic FlameCoat Systems as PF200 was used with the addition of a fluidized bed powder delivery system. Polymer coatings were sprayed to a thickness of approximately 800 micrometers (30 mils) at a temperature of 218-232 °C (425-450 °F).

---

\* comminution: reduction of a material to a powder.

### ***Microstructural Analysis***

The cross-section of the as-sprayed PCCP coating is shown in Figure 13. Contrast is observed in the cross-section due to the various polymer chemistries, sizes, and pigments originally used in the processing. Polymer particles impinging upon the substrate (preheated to 77 °C [170 °F]) are either semi-molten or fully molten. Upon impact, the polymer droplet (splat) will spread, deform, and coalesce to the substrate or underlying topography. The lower melting point polymers such as low density polyethylene will have a lower melt-viscosity than higher molecular weight formulations, and thus will flow more easily. Spherical splats are also observed in the microstructure representing insufficient particle melting.

Due to the large differences in surface tension between different polymeric species in the PCCP blend, limited diffusion can occur between incompatible splats. Recent studies have also shown the need for proper melt-compatibilization to improve the cohesive strength between immiscible polymers [18, 19, 20]. Table 4 lists the critical surface tensions, solubilities, and thermal properties for the polymers making up PCCP. The polymer combination with the least compatibility is polyethylene with polyethylene terephthalate.

The surface of the as-sprayed PCCP coating is shown in Figure 14. Thin macroscopic cracks, of lengths up to 800 micrometers, propagated along consecutive splat boundaries. Interfacial boundaries between incompatible polymer species, in conjunction with differences in thermal expansion behavior is most likely responsible for inducing the cracks between neighboring splats during cooling.

### ***Accelerated Degradation***

The QUV accelerated weathering tester simulates the damaging forces of sunlight and rain. Coatings were exposed to 4 hours UV-B light at 60 °C and 4 hours condensation at 50 °C for a total of 1250 hours. Deterioration to the surface includes cracking, chalking, and photo-bleaching. The extent of these distresses depends upon the volume fraction of EMAA blended with the PCCP. Figure 15 shows weathered surfaces of 100 percent PCCP, 50 percent PCCP, 25 percent PCCP, and 100 percent EMAA. Figure 16 depicts the dominant crack propagation paths.

For the case of 100 percent PCCP, both the unmelted and melted PCCP particles have poor interfacial adhesion to the surrounding matrix, resulting in interfacial debonding. Cracks were observed with lengths of up to 1600 micrometers. These longer cracks seem to propagate tangentially from the particle, in the direction of the interfacial disbondment. Cracks shorter in length also initiated radially from

the particle/matrix interface. The 75 percent PCCP coating appeared similar to the 100 percent commingled case, but the interfacial zone between particle and surrounding polymer was slightly narrower. Radial cracks from one particle or splat intersected other radial and tangential cracks from neighboring particles. The PCCP particles are distributed farther apart in the 50/50 mixture, thus decreasing the number of crack intersections. Unmelted particles are discernible, but they are clearly embedded within the surrounding matrix. Radial cracks from one particle often propagated the distance to surrounding incompatible polymer splats. At a 25 percent PCCP volume fraction, only radial cracks were observed to propagate from the PCCP/EMAA interface, and inter-particle cracking was not evident. Cracks were not observed for the pure EMAA coating, but photo-bleaching was evident, resulting in a loss of gloss.

The cracking was measured to quantify the extent of degradation to the PCCP blends. A pseudo crack density index was determined using a five-line intercept method (Figure 17). The error bars represent the standard deviation from measuring triplicate samples. The number of cracking events decreased as the percentage of virgin EMAA copolymer in the blend was increased. The 75 percent PCCP blend had approximately the same crack density as the pure commingled polymer. The 25 percent PCCP blend had a crack density index of 0.3 cracks/mm (3 cracks/cm). Crack length distributions were also determined for each coating system using optical microscopy, and the average crack length was plotted in Figure 18. Each sample had a large distribution of cracks, and therefore had a large standard deviation. However, the overall trend suggests that increasing the volume percentage of EMAA in the blend decreases the average crack length. These numbers do not include cracks smaller than 10 micrometers, which were later observed using scanning electron microscopy.

### ***Adhesion of PCCP and Blends***

In order to assess coating adhesion to steel, the standard ASTM C633 protocol was modified. It was previously found that epoxy does not bond well to thermoplastic surfaces primarily due to low surface energies. The tensile adhesion test stud was, therefore, abrasive-blasted to 10 micrometers, heated to 204 °C (400 °F) and then placed on the coating with a force of 350 g. This allowed the stud to be fusion bonded to the coating surface. The circumference of the stud was also scribed to bare metal to eliminate the possibility of shear forces being distributed to adjacent polymer during the test. The hydraulic Instron used a constant strain rate of 0.0005 in/sec (approximately 0.0013 cm/sec) and the force required to remove the coating was recorded.

Unblended PCCP and PCCP blends with EMAA copolymer were sprayed to the same thickness (30 mils) onto steel substrates with a 10 mil anchor profile. The tensile adhesion strength was measured before and after weathering (Figure 19). The data points reflect an average strength derived from five measurements. Failure mechanisms changed from 100 percent adhesive (for the 100 percent PCCP coating) to 100 percent cohesive failure (for 100 percent virgin EMAA) as the percentage of EMAA increased in the commingled polymer coatings. The weathering-induced cracking did not significantly affect the adhesive properties of the applied coatings. Rust was also evident on the steel surface from which the 100 percent PCCP coating was removed, signifying water penetration. It can be concluded from the data that the adhesion to steel increases as the volume percentage of EMAA in the PCCP blend increases.

#### ***Discussion of PCCP Flame Spray Tests***

Microstructures of as-sprayed PCCP coatings show evidence of cracking. Accelerated weathering induced further cracking, photo-bleaching, and a higher surface roughness. The PCCP powder was blended with ethylene methacrylic acid copolymer in ratios of 25 percent, 50 percent and 75 percent by volume. Introduction of the EMAA was shown to decrease the weathering-induced crack density as well as reduce the average crack length. Cracking was not evident in the 100 percent EMAA coatings. Blending EMAA copolymer with PCCP also increased the adhesion to steel from 250 psi for 100 percent PCCP to 1100 psi for 25 percent PCCP. Accelerated weathering did not appreciably affect coating adhesion. Using unmodified post-consumer commingled polymer in volume fractions less than 25 percent may promote significant materials and waste disposal cost savings, but not without a sacrifice in coating cohesion.

## **Mechanical Properties of Polymer Materials and Blends**

### ***EMAA Copolymer***

The purpose of this study was to determine the tensile properties of spray-formed coatings and determine whether pigment or cooling rate affects these properties. Two EMAA copolymer powders were chosen, having melt flow indices of 500 g/10 min (PF113) and 32 g/10 min (PF111). As previously discussed, coatings were sprayed onto a Teflon<sup>®</sup> coated skillet that was preheated to 66 °C (150 °F). Once cool, the deposit is easily removed and stamped to the ASTM D 632 type IV dog-bone geometry. Table 5 summarizes the average secant modulus (Young's

modulus), yield strength, yield strain, tensile strength, elongation to break, and toughness values obtained for each EMAA coating system.

When PF111-clear was deposited at 160 °C (320 °F), the splats had not completely coalesced, resulting in a rough surface. The tensile strength, elongation to break, and toughness were considerably lower than coatings deposited at 216 °C (420 °F), however, the modulus and yield strength were not appreciably different. During testing, a neck forms at the yield point and then propagates over the gauge length. Thus, PF111 coatings at 160 °C cannot plastically deform due to lower splat cohesion in comparison to coatings sprayed at 216 °C. A smooth surface was apparent without visible porosity for PF111 at 216 °C. In addition, coatings elongated to approximately 800 percent elongation before failure. Since this polymer strain hardens (Figure 20) the tensile strength increases with increasing strain. The presence of pigment increased the modulus and yield strength only slightly, but the pigment also reduced the elongation to break decreasing both the tensile strength and the toughness. When unpigmented PF111 was sprayed at 216 °C and quickly quenched into water at 15 °C, a highly transparent coating was produced. In comparison to normal cooling (Figure 21) the quenched sample had a lower modulus, lower yield strength, higher tensile strength, higher elongation to break, and higher toughness. These data suggest that the crystallinity and the density had decreased, resulting in a more open structure, thus decreasing the modulus. The elongation may have increased due to fewer entanglements, resulting in greater chain orientation during tensile testing. The tensile strength increases with increasing elongation to break due to strain hardening. When PF111 unpigmented coatings were sprayed at 271 °C (520 °F), the coatings appeared yellowish in color due to an increase in oxidation products. Spraying at this temperature also induced visible porosity in the coatings resulting in 100-500 micrometer bubbles. These bubbles effectively reduce the cross-sectional area, explaining the decreased modulus, yield strength and tensile strength. Interestingly enough, the bubbles deformed in the direction parallel to the applied stress and did not reduce the elongation to break; thus, only a minor sacrifice in toughness was observed.

The copolymer PF113 was also sprayed at various processing conditions. PF113, which has a higher melt flow index than PF111, results in a coating that has a lower modulus, lower yield strength, lower tensile strength, lower elongation to break, and lower toughness than PF111 coatings. The shape of the stress-strain curve is quite different as well, due to the lack of strain hardening. Once the yield point is reached, the tensile strength essentially remains constant during necking. However, when PF113 was water-quenched at 160 °C, not only did the elongation to break increase, but the molecular architecture changed due to the observed strain hardening effect (Figure 22). Since PF113 has a higher melt-flow index, and

thus a lower molecular weight, coatings could be deposited at lower temperatures. Mechanical properties improved as coating temperatures increased from 104 to 160 to 216 °C. Once again, the modulus and yield point did not differ at these temperatures, implying that only plastic deformation is dependent upon the microstructure. Pigment slightly influenced the modulus and strength, but did decrease the elongation to break. Figure 23 summarizes the properties of various PF113 coatings deposited at 160 °C.

### ***Recycled PCCP Blends***

Post-consumer commingled plastic coatings and blends were sprayed with the Plastic FlameCoat 400 torch with gravity feed. The PCCP powder was previously melt-compounded and screened to a -50 mesh. EMAA copolymer powder (PF111-pigmented) was mechanically blended in a salt-and-pepper mixture in increments of 10 percent by volume. As the composition varied from 0 to 100 percent PCCP, coatings were deposited at increasing temperatures, ranging from 204 °C (400 °F) at 0 percent PCCP to 232 °C (450 °F) at 100 percent PCCP loading. Table 6 outlines the mechanical properties of such blends and Figure 24 depicts the stress-strain curves for each mixture. Since the matrix phase varied from 0 to 100 percent, the entire spectrum is represented, i.e., elastomeric particles dispersed in a brittle matrix and reinforcing particles in an elastomeric matrix. Each mechanical property was then plotted as a function of EMAA loading (Figure 25). Although 100 percent PCCP coatings have a higher modulus and greater tensile strength than 100 percent EMAA coatings, PCCP coatings do not have much ductility. A 10 percent addition of PCCP decreased the elongation to break from 637 percent to 114 percent. This effect reduces coating toughness from 8868 lb/inch to 1354 lb/inch. The secant modulus increased linearly with increasing PCCP content. In addition, tensile strengths increased with increasing PCCP contents up to 70–80 percent PCCP. The tensile and yield strengths did not change with further PCCP loadings. The lowest tensile strength corresponded to a 10 percent addition of PCCP. This 10 percent inclusion had the additional affect of preventing the EMAA copolymer to strain harden during extension. This also explains why the yield strength data show a different trend than the tensile strength data at low PCCP loadings.

### ***Discussion of Mechanical Properties Findings***

The mechanical properties of combustion-sprayed polymers depend upon the processing parameters. The processing parameters determine coating temperatures which, in turn, affect the polymer microstructure. If the deposition temperature is too low (104 °C for PF113 and 160 °C for PF111), coatings have low strengths, low elongation ratios, and low toughness values. Increasing the coating temperature

allows the particles to fully coalesce, resulting in maximized strength and toughness. However, at 271 °C, PF111 had visible porosity, which decreased the strength and modulus of elasticity. Pigment acts as reinforcement in the sense that the modulus increased. However, the elongation to break decreased, reducing overall coating toughness. It is believed that water quenching decreases the crystallinity, resulting in a lower elastic modulus and yield strength, but higher elongation to break.

Coating toughness was decreased by blending PCCP with EMAA copolymer. The decrease in toughness and elongation to break was accompanied by an increase in strength and elastic modulus. Since PCCP contains approximately 80–90 percent polyethylene and EMAA is a functionalized polyethylene, some compatibility is expected to exist.

## EMAA Adhesion to Steel

### *Peel Strength*

In order to assess the polymer adhesion to steel, a 90 degree peel test was constructed according to ASTM D 3167 specifications, as previously discussed. Such tests allow the determination of the localized bond strength at the coating /substrate interface [21-23]. The measured peel force is the sum of the force required to mechanically bend the coating and the force to break secondary bonds at the interface. The force required to propagate a crack of width equal to the specimen width is recorded on a digital data acquisition board at a rate of 8 measurements per second.

The significance of molecular weight on adhesion was investigated by comparing two formulations of EMAA—PF111 and PF113—having melt flow indices of 32 and 500 g/10 min. The copolymers were obtained from Plastic FlameCoat, Inc. as PF111 and PF113, respectively. The virgin EMAA powders were flame sprayed with a Plastic FlameCoat 200 gun 7, using propane and compressed air as the fuel gasses. The spray conditions were chosen to fully coalesce the particles well within pyrolysis limits as determined from the previous studies. The influence of substrate topography on peel strength was ascertained by spraying steel substrates under the following surface preparation conditions: polished, abrasive-blasted to an Ra of 10 micrometers, and the as-received condition.

Figure 26 summarizes the average peel strengths for PF113 and PF111 as a function of steel topography [24]. The peel strength values reflect the averaged

force required to separate the two surfaces, which includes the energy dissipated by plastic deformation. Higher peel strengths were observed for the higher molecular weight EMAA copolymer for each steel surface profile. The peel adhesion strength increased fourfold for PF113 upon abrasive-blasting the as-received steel and increased by a factor of two for PF111. Peel strengths also increased (for both formulations) by approximately  $1000 \text{ J/m}^2$  upon polishing the as-received steel.

### ***Polished Steel***

The peeling fracture mechanisms were dependent upon the substrate topography. In a series of experiments designed to determine the effect of topography on the performance of the coatings, EMAA copolymer was applied to polished steel, abrasive-blasted steel, and on steel as received from the supplier. The EMAA copolymer coatings on polished steel show unstable crack propagation, as evident by the sawtooth load-displacement curves in Figure 27. Such behavior was observed for both PF111 and PF113 materials, but a greater force was required to propagate and bring the crack to rest for PF111. The peaks on the load-displacement plot correspond to crack initiation and the valleys correspond to crack arrest. This implies that the crack accelerates faster than the strain rate,  $6 \text{ mm/sec}$ , and the strain energy release rate,  $G$ , is larger than the interfacial fracture toughness,  $\Gamma^5$ . The crack continues to propagate until the strain energy release rate is balanced by the increase in fracture surface area.

The fracture mechanism is referred to as “slip-stick” failure. Polymer was extracted from the coating creating a series of parallel band markings on the surface of the polished steel. Examination of the polymer surface from which the polymer was extracted also reveals band markings (Figure 28). However, using higher magnification, the markings on the polymer surface actually represent a series of crack networks. Not only did the position of the band markings coincide between the polymer coatings and the respective steel substrates, but their position also corresponds to the minima on the load-displacement plot. Polymer material was only found within the discrete band locations on the steel surface, signifying that splat decohesion did not take place during crack propagation. The distance between the markings for both PF111 and PF113 increased linearly from  $1 \text{ mm}$  to approximately  $5 \text{ mm}$  during the test. This was observed by measuring the distance between the markings on the steel surface and was verified by measuring the distance between peak minima. This suggests that a greater amount of energy is absorbed and subsequently released as kinetic energy as the displacement increases.

### ***Abrasive-Blasted Steel***

Polymer strips peeled from an abrasive-blasted surface with a surface roughness,  $R_a$ , of 9 micrometers failed in a different manner. As evident in Figure 29, the output does not show the same degree of load deflections that occurred upon peeling from polished steel. In addition, polymer band markings were not observed on the surface of the roughened steel nor on the coating. Examination of the polymerside of the interface (post-peeling) revealed a highly deformed surface. In fact, the higher molecular weight polymer coating (PF111) showed a greater amount of deformation than PF113. In addition, a greater peel force was recorded for PF111. Holes on the surfaces of both coatings were evident, surrounded by a plastically deformed rim (Figure 30). These holes signify splat decohesion from the matrix since the holes are about the same size as a splat (approximately 100 micrometers). It appears that the matrix attempted to constrain the splat but failed. Polymer fibrils were often observed near the perimeter of such holes. Examination of the abrasive-blasted steel surface revealed that polymer material was clearly anchored within the undulations (see Figure 31). The polymer within the steel topography was also elongated to a fibrous geometry. This suggests that the polymer was sufficiently anchored to the steel to allow a filament to be formed and ultimately withdrawing the particle from the coating. A fibril or filament near a hole on the polymer surface may actually be the remains of a splat after extension and subsequent rupture. A distribution of polymer was found on the abrasive-blasted steel surfaces for both PF111 and PF113 coatings.

It is apparent that a different fracture mechanism is taking place than peeling on a polished surface. This failure can therefore be characterized as exhibiting greater crack stability, although minor load deflections were visible on the load-displacement plots. The energy available for crack propagation is utilized as fracture surface energy as well as the energy required to extract the splat from the coating. The minor load deflections may possibly be attributed to the extension of the polymer splat from the coating to the steel surface. A load drop would then correspond to the final stage of splat decohesion. Slip-stick failure could not take place because work was constantly required to remove the mechanically anchored polymer from the steel topography. This extra work is reflected in the higher peel force (for both EMAA formulations) to remove the coating from abrasive-blasted steel as compared to removing a coating from a polished steel surface.

### ***As-Received Steel***

The as-received steel specimens contained an undetermined amount of embedded grease and various amounts of surface oxidation. Failure mechanisms were

dependent upon the extent of surface contamination. All low molecular weight EMAA specimens (PF113) peeled in a stable fashion (no load deflections), fracturing near the interface. Fracture of the higher molecular weight EMAA (PF111) was dependent upon the location of the surface staining. Regions of the steel containing embedded grease displayed stable crack propagation. The contamination was observed on the peeled strip as well. However, areas with less surface staining displayed failure mechanisms characteristic of slip-stick, with accompanying band marks on the steel as well as load deflections on the output (Figure 32a). It is not known what concentration of contamination is required to change the crack front stability.

Contamination from the as-received steel was found on both PF113 and PF111 polymer coatings (Figure 32b). The peeled polymer surfaces showed significantly less deformation than coatings peeled from abrasive-blasted surfaces. However, holes were observed on the peeled surface adjacent to the removed contamination. Thus, the adhesion to an as-received steel surface was sufficiently strong to remove some polymer material from the coating. Polymeric splats and filaments were thus observed on the as-received steel surface. Although the polymer will adhere to surface oxides, maximum adhesion is achieved by removing surface contamination and abrasive-blasting the surface to a rough profile. Contaminants and oils will decrease the interfacial interactions between the polymer and steel surface, thus, decreasing the interfacial adhesion.

### ***Interfacial Bonding***

As previously noted, the experimentally measured peel force is the sum of the forces required to mechanically bend the coating and those required to break the interfacial bonding. This interfacial adhesion is dependent upon the number of atomic bonds per unit area multiplied by the atomic bonding energy. In the absence of primary bonding, Lewis acid-base interactions provide a mechanism for tenacious interfacial bonding. Fowkes has reported such bonding between various polymers and substrate materials [25, 26].

One hypothesis can be based upon examination of the polymer chemistry. The carbonyl moiety, stemming from the carboxyl group, may act as a nucleophile thus capable of donating electron density (Lewis base) to the surface of steel. The surface of steel is hydroxylated to some degree and will accept the electron density since hydrogen is partially positive (Lewis acid). Hydrogen bonding is therefore a subset of Lewis-acid base reactions. Figure 33 illustrates the proposed secondary bonding interactions between EMAA and the steel substrate. It should be noted

that a similar model for cohesion is plausible since the carbonyl group of one polymer chain may attract the hydroxyl group of another chain.

Abrasive-blasting the steel surface increases the surface area and provides increased mechanical anchoring. The surface energy is also expected to increase due to bond deformation. A monolayer of oxidation products will form within minutes of abrasive-blasting and thus contribute to interfacial bonding. However, porosity may result if polymer is sprayed onto oxide layers greater than a few monolayers in thickness. Air trapped by oxidation products on steel can diffuse into the polymer, creating voids of millimeter dimensions. Interfacial porosity provides a path for crack propagation and thus decreases the interfacial fracture toughness. On as-received steel surfaces, contamination includes both embedded dirt and machining oil. Oils are nonpolar and do not provide a site for tenacious bonding. Embedded dirt and oils act as a lubricant and decrease the interfacial interactions between the steel and the polymer. This hypothesis is supported by the interfacial failure mechanism exhibited by a heavily contaminated surface.

#### ***Discussion of EMAA Adhesion Findings***

The ASTM D 3167 peel test is not suitable for evaluating PCCP blends due to their lower strength and ductility, but it is quite useful in assessing the adhesion of flame-sprayed EMAA coatings to various steel surfaces. The copolymer PF111 is of higher molecular weight and density than PF113 and required a greater load to propagate an interfacial crack. An abrasive-blasted surface produced the strongest joint, followed by polished steel and then the as-received steel surface. It is therefore recommended to abrasive-blast the steel surface for maximum coating adhesion.

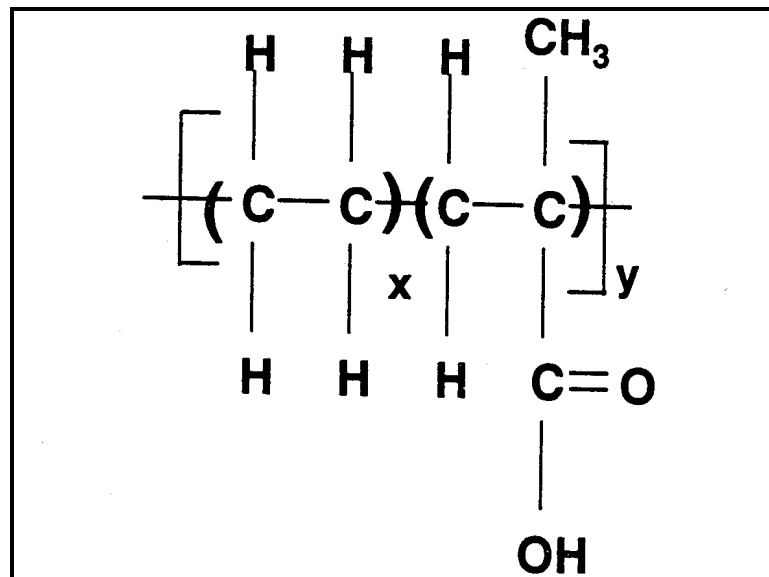


Figure 5. Ethylene methacrylic acid copolymer powder.

Table 1. Thermal-spray parameters for design of experiments study.

Fixed Parameters	Variable Parameters
Propane tank pressure : 41 kPa	Powder feed rate: 70 g/min and 140 g/min
Nitrogen tank pressure: 345 kPa	Standoff distance: 25 cm and 50 cm
Compressed air pressure: 827 kPa	Substrate preheat temp: 21 °C and 87 °C
Robotic traverse speed: 25 cm/sec	Propane flow rate: 6.6 l/min and 15.1 l/min
Spray step distance: 3 cm	Compressed air rate: 120 l/min and 200 l/min

Table 2.  $2^{5-1}$  design for EMAA copolymer.

Specimen Number	Powder Feed Rate	Standoff Distance	Substrate Preheat Temp	Propane Flow Rate	Air Flow Rate	Response 1	Response 2	Response 3
	$X_1^*$	$X_2$	$X_3$	$X_4$	$X_5$	$Y_{\text{temperature}}$	$Y_{\text{roughness}}$	$Y_{\text{E.R.}}$
	(g/min)	(cm)	°C	(l/min)	(l/min)	Deposit Temperature (°C)	Surface Roughness ( $\mu\text{m}$ )	Splat Elongation Ratio
1	70	25	21	6.6	200	60	40	2.06
2	140	25	21	6.6	120	74	22	2.85
3	70	50	21	6.6	120	69	28	4.81
4	140	50	21	6.6	200	96	10	5.13
5	70	25	87	6.6	120	118	20	4.02
6	140	25	87	6.6	200	151	12	4.33
7	70	50	87	6.6	200	121	50	1.59
8	140	50	87	6.6	120	157	10	5.49
9	70	25	21	15.1	120	78	43	2.33
10	140	25	21	15.1	200	108	16	3.85
11	70	50	21	15.1	200	77	48	2.20
12	140	50	21	15.1	120	119	8	5.40
13	70	25	87	15.1	200	160	11	4.21
14	140	25	87	15.1	120	151	11	3.53
15	70	50	87	15.1	120	171	11	4.73
16	140	50	87	15.1	200	182	3	7.33
17	125	38	54	10.9	160	129	13	5.03
18	125	38	54	10.9	160	138	11	4.98
19	125	38	54	10.9	160	131	9	5.98

\* The  $X_1$  to  $X_5$  and  $Y_{\text{temperature}}$ ,  $Y_{\text{roughness}}$ , and  $Y_{\text{E.R.}}$  refer to the variables and responses used in the empirical modeling within the text.

Table 3. Statistically significant parameters\*.

Deposit Temperature (°C)	Surface Roughness ( $R_a$ in micrometers)	Splat Elongation Ratio
Substrate Temperature <i>Effect = 66</i>	Powder Feed Rate <i>Effect = 20</i>	Powder Feed Rate <i>Effect = 1.5</i>
Propane Flow Rate <i>Effect = 25</i>	Substrate Temperature <i>Effect = 11</i>	Standoff Distance <i>Effect = 1.2</i>
Powder Feed Rate <i>Effect = 23</i>	Substrate Temperature / Propane Flow Rate <i>Effect = 9</i>	Powder Feed Rate / Compressed Air Rate <i>Effect = 1.2</i>
	Powder Feed Rate / Standoff Distance <i>Effect = 7</i>	Powder Feed Rate / Standoff Distance <i>Effect = 1.0</i>
		Substrate Temperature <i>Effect = 0.83</i>

\* The process parameters are presented in descending order of influence.

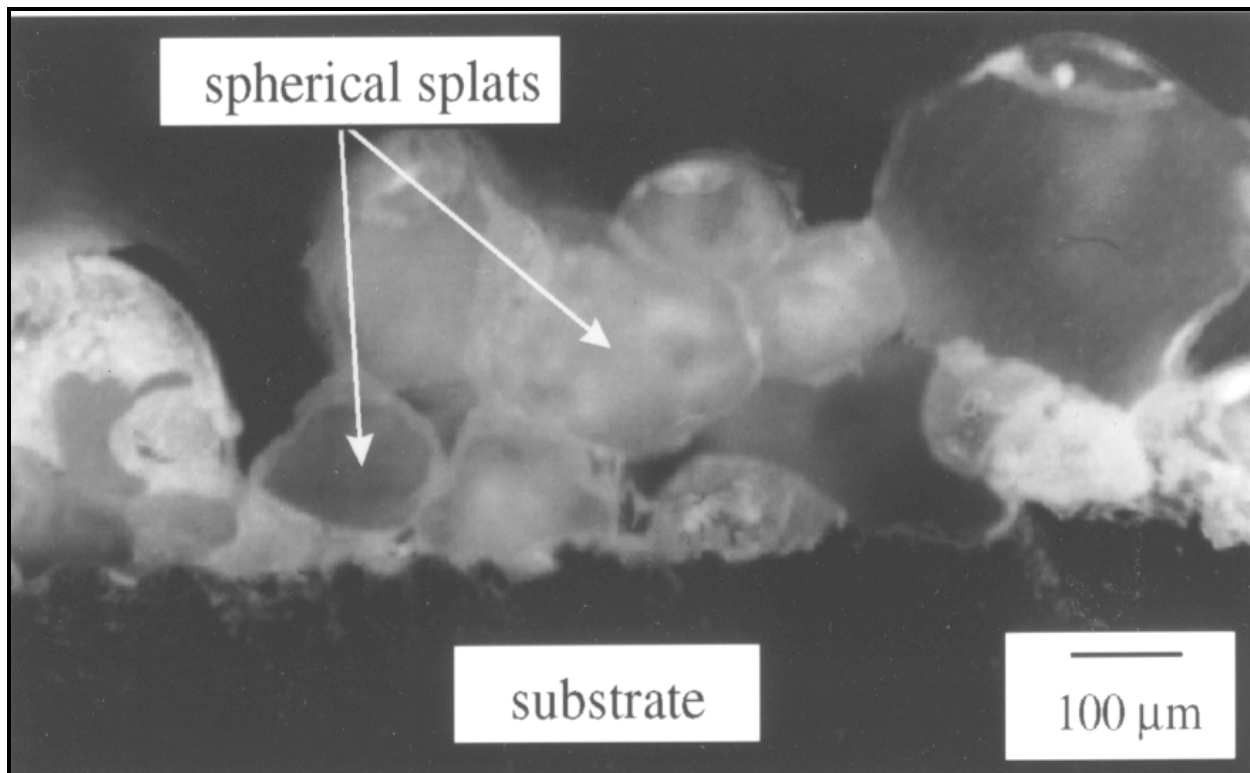


Figure 6. Cross-section of coating with low splat elongation ratios.

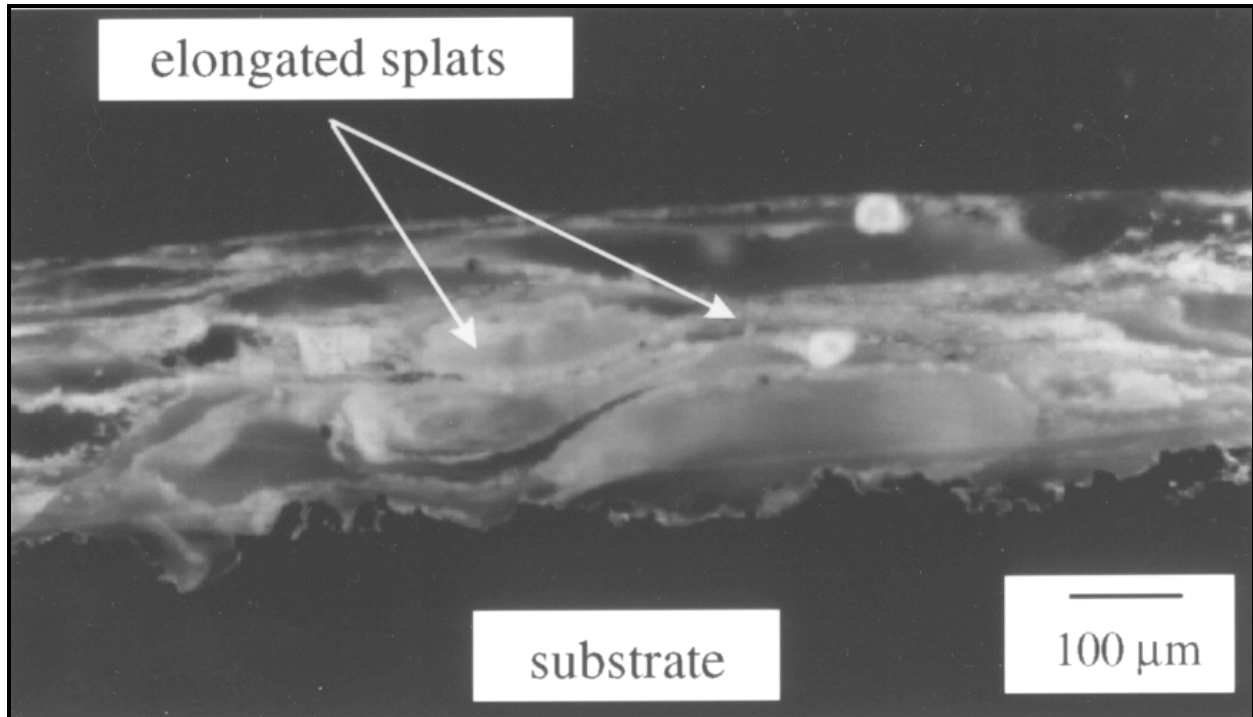


Figure 7. Cross-section of coating with high splat elongation ratios.

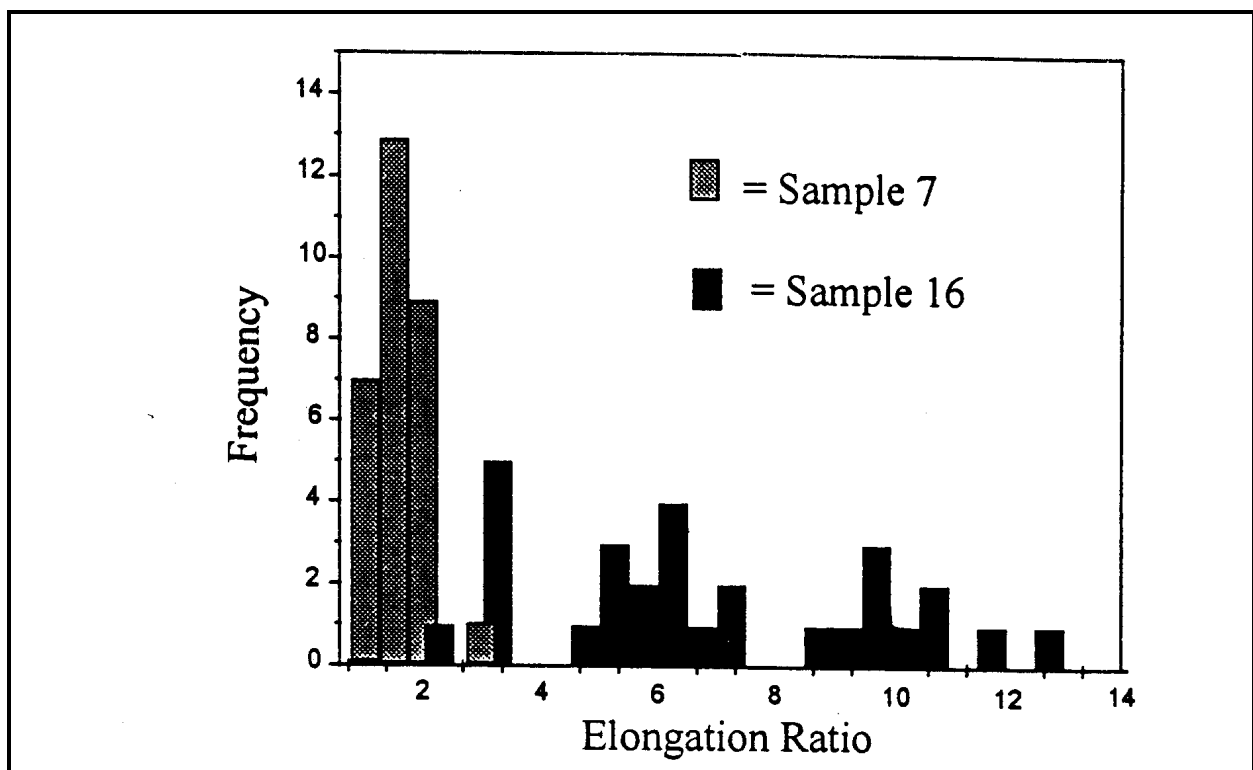


Figure 8. Distribution of elongation ratios for the microstructural extremes.

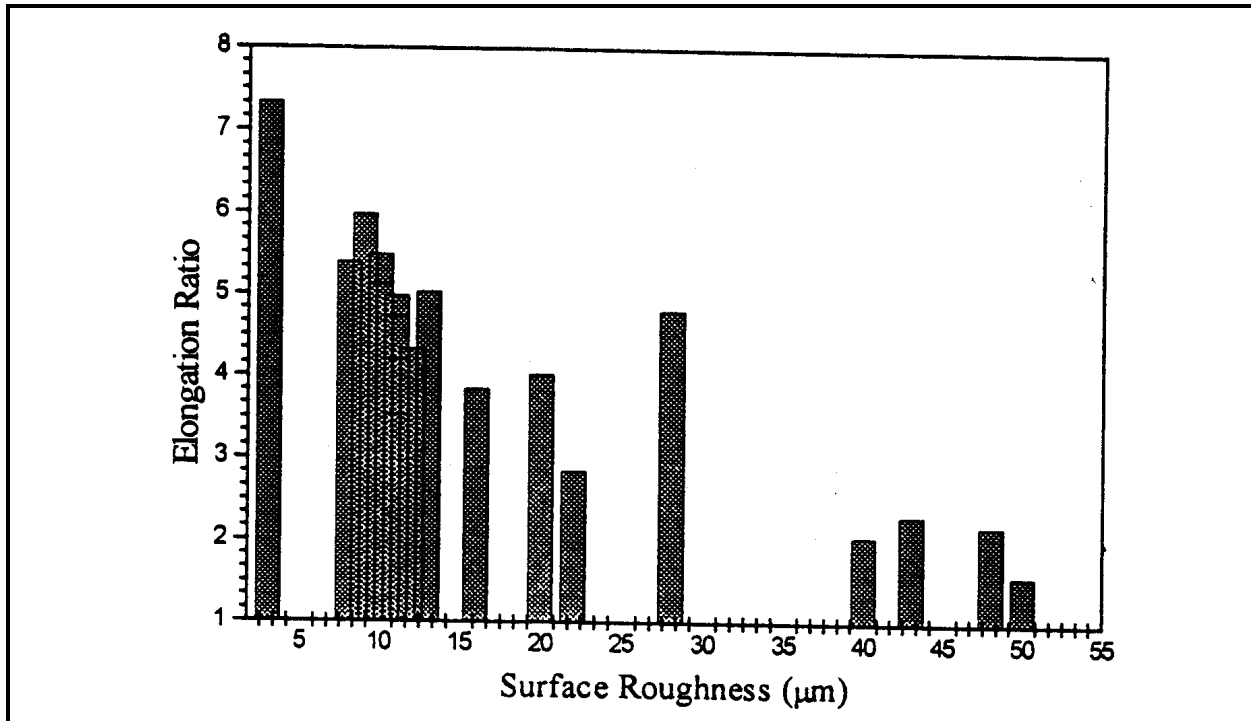


Figure 9. Relationship between elongation ratio and surface roughness.

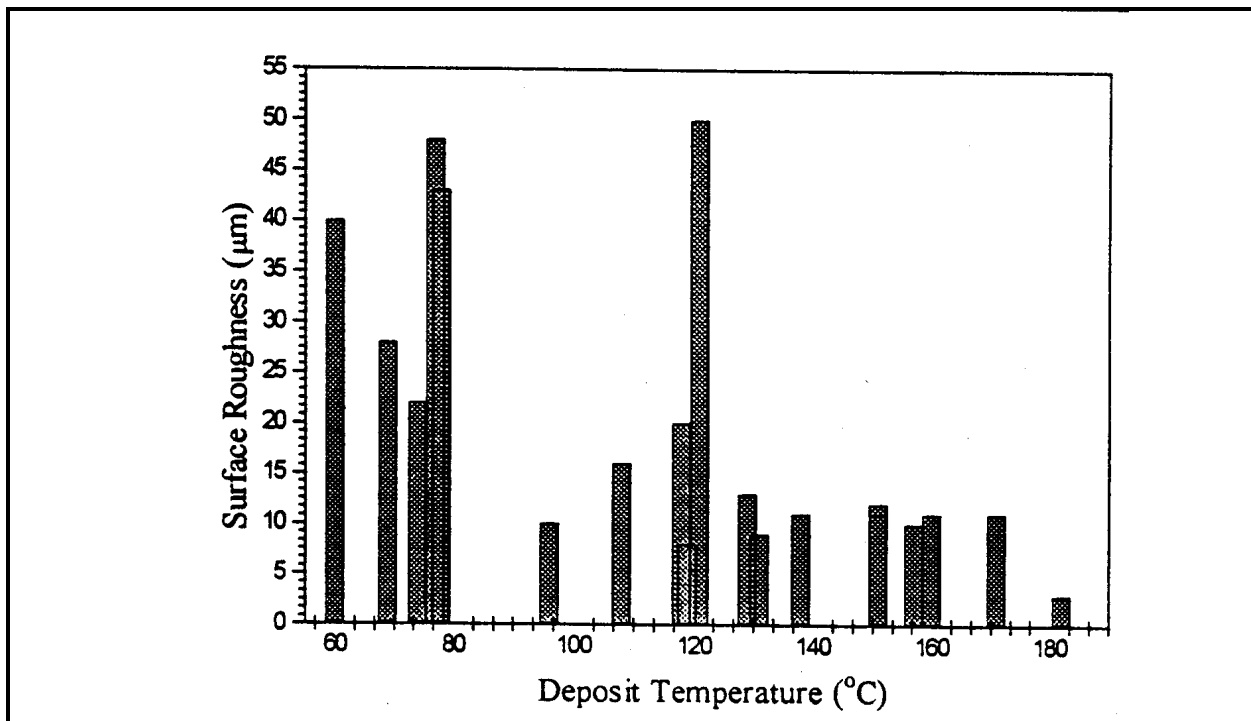


Figure 10. Relationship between surface roughness and deposit temperature.

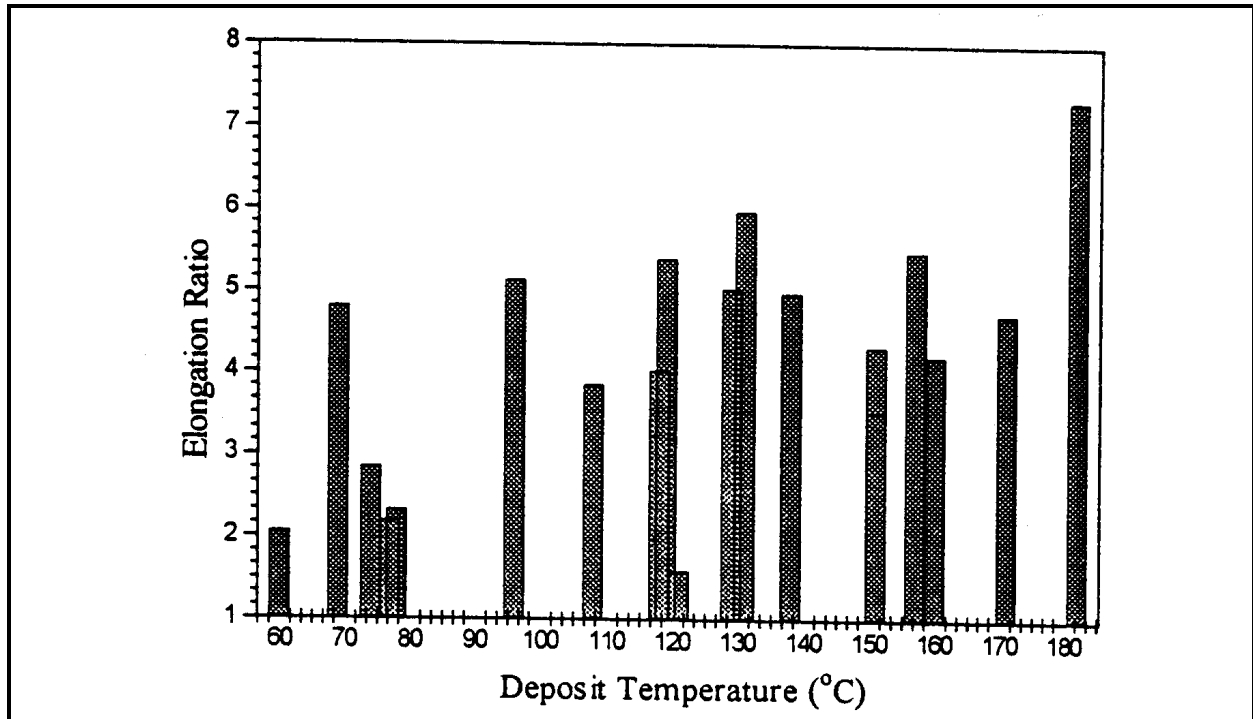


Figure 11. Relationship between splat elongation ratio and deposit temperature.

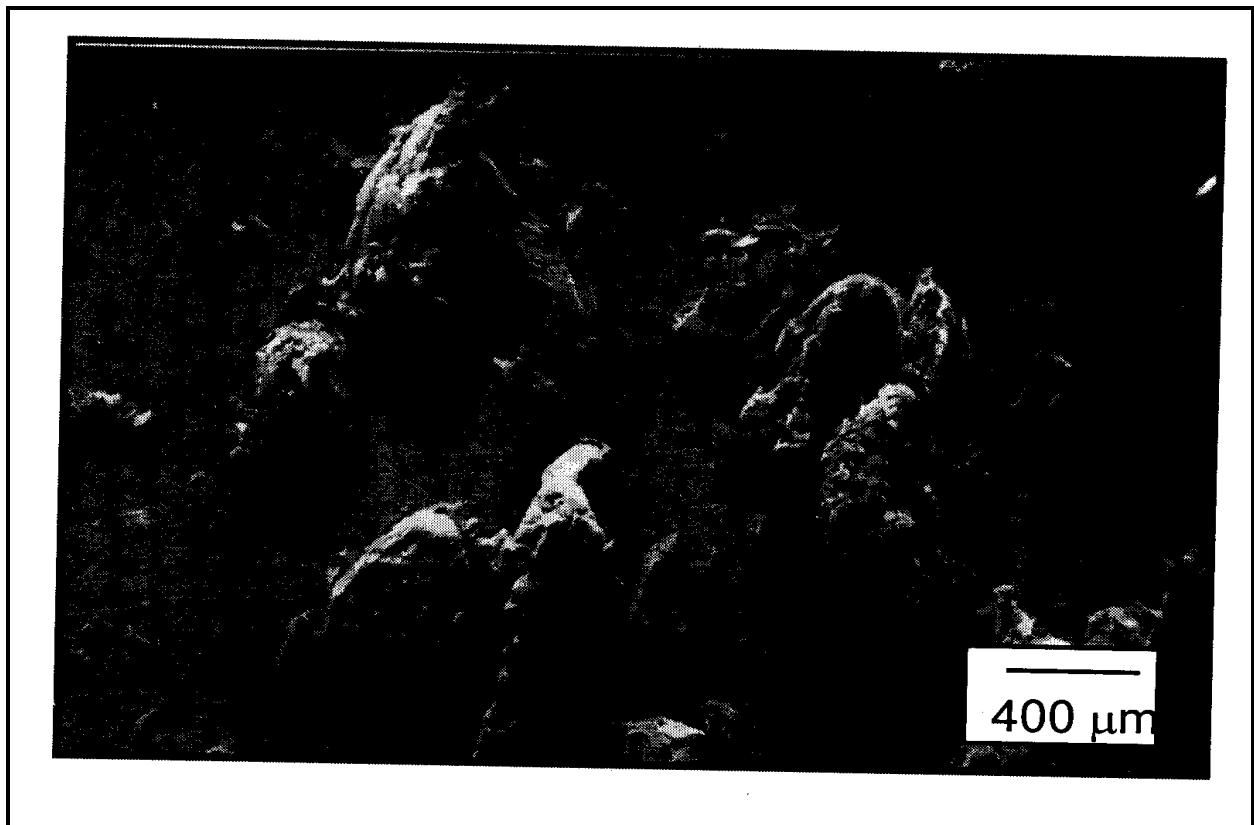


Figure 12. Morphology of post-consumer commingled plastic after grinding.

Table 4. Bulk properties of individual polymer constituents.

Polymer	Glass Transition Temperature (°C)	Critical Surface Tension (mN/m at 20 °C)	Solubility Parameter $10^3 [J/m^3]^{1/2} 10^{-3}$	Thermal Conductivity (cal/s-cm-K)
Polyethylene	-80 – -90	32–34	16–17	8–12
Polypropylene	-18	34	19	2.8
Polystyrene	100	33	17–19	2.4–3.3
Polyvinylchloride	81	40	19–20	3.5–5.0
Polyethylene terephthalate	70	43	22	
*Ethylene Methacrylic Acid Copolymer	-50	44		5.8

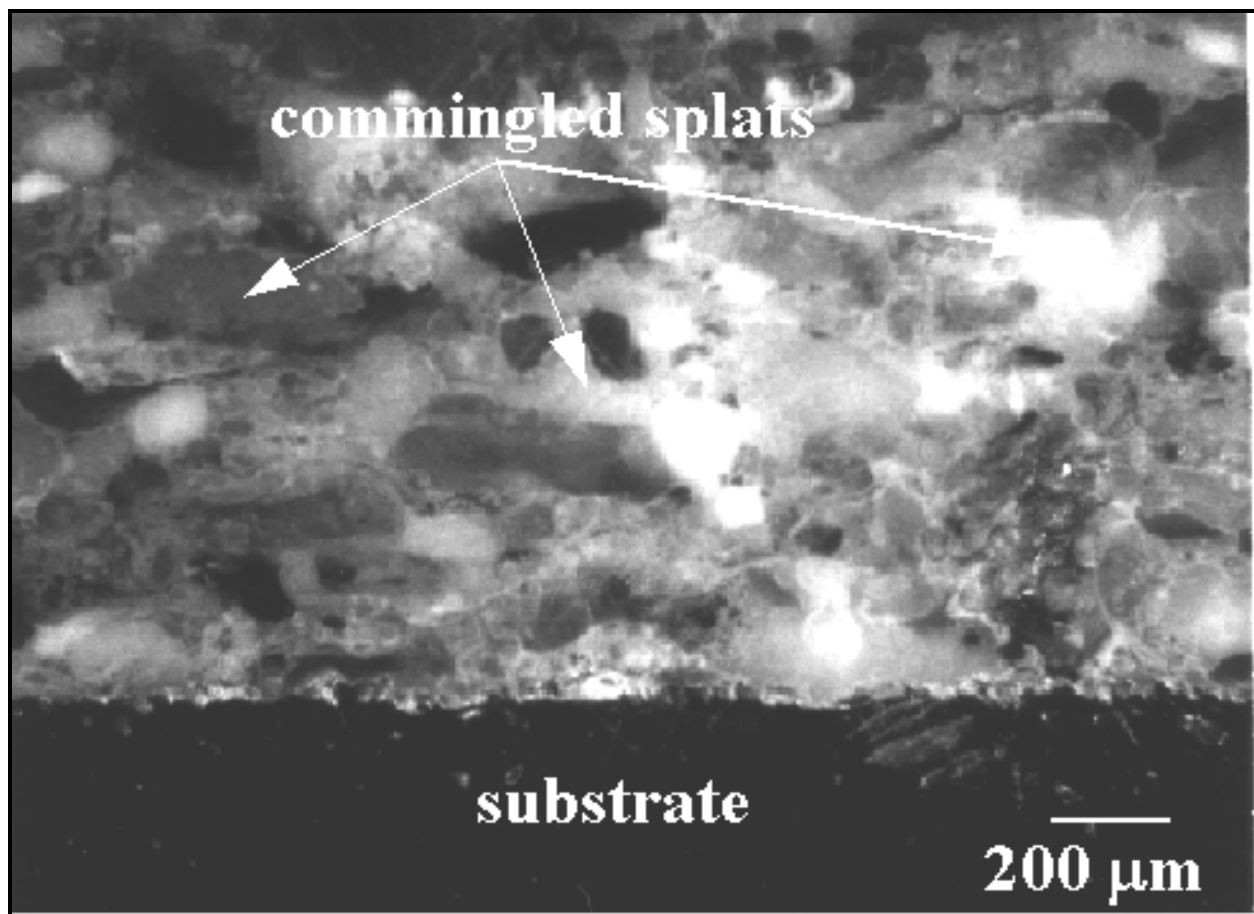


Figure 13. Cross-section of post-consumer commingled polymer coating.

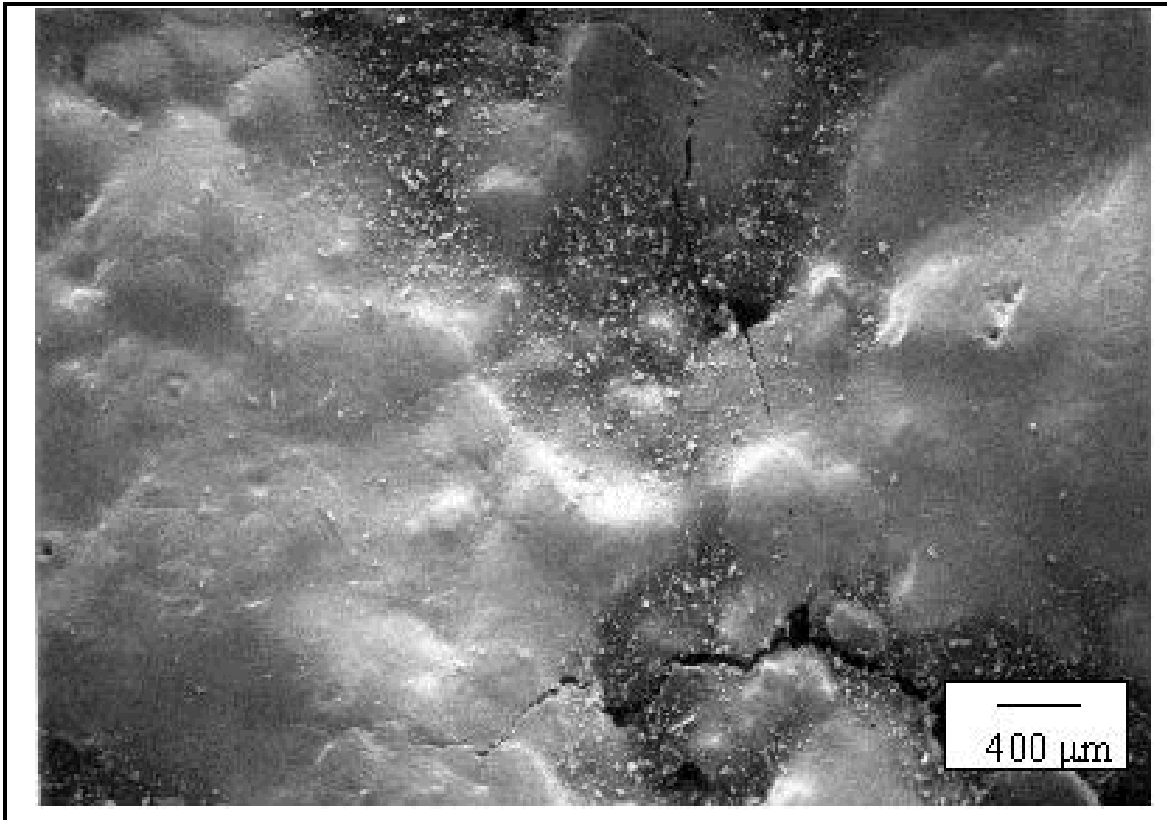


Figure 14. Surface of as-sprayed PCCP coatings from dry compounded recycled plastic.

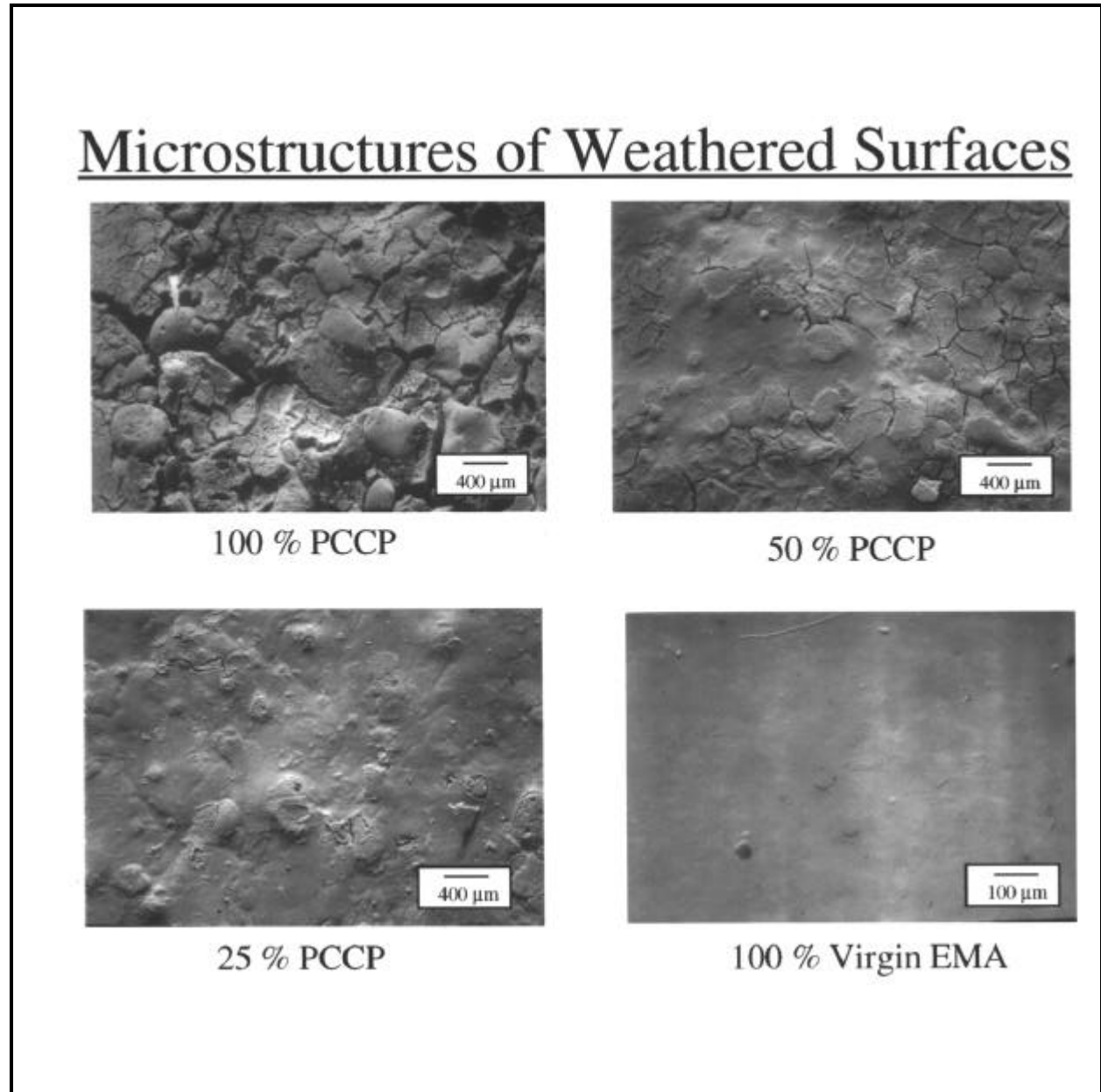


Figure 15. Surfaces of weathered polymer coatings.

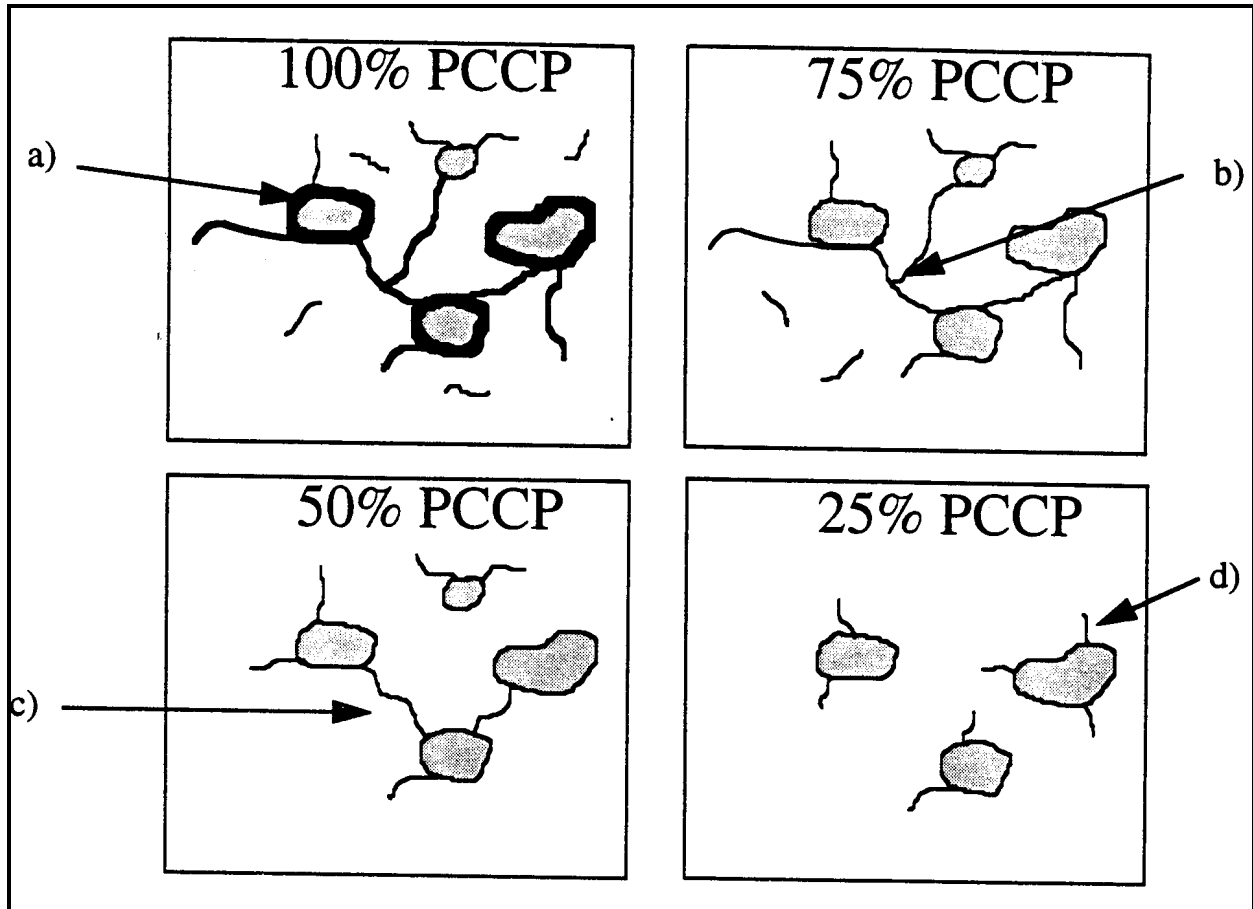


Figure 16. Cracking mechanisms for recycled post-consumer commingled polymer blends: (a) interfacial debonding, (b) crack intersection, (c) inter-particle cracking and (d) radial cracking.

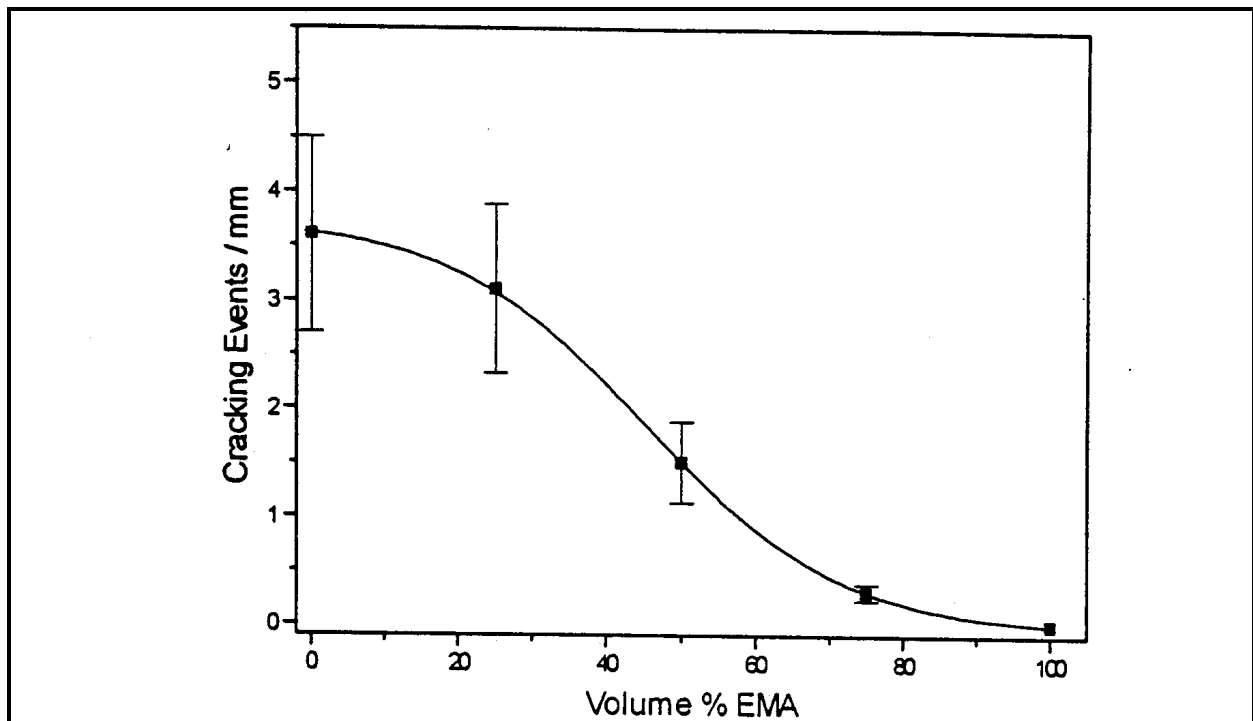


Figure 17. Pseudo crack density of exposed coatings.

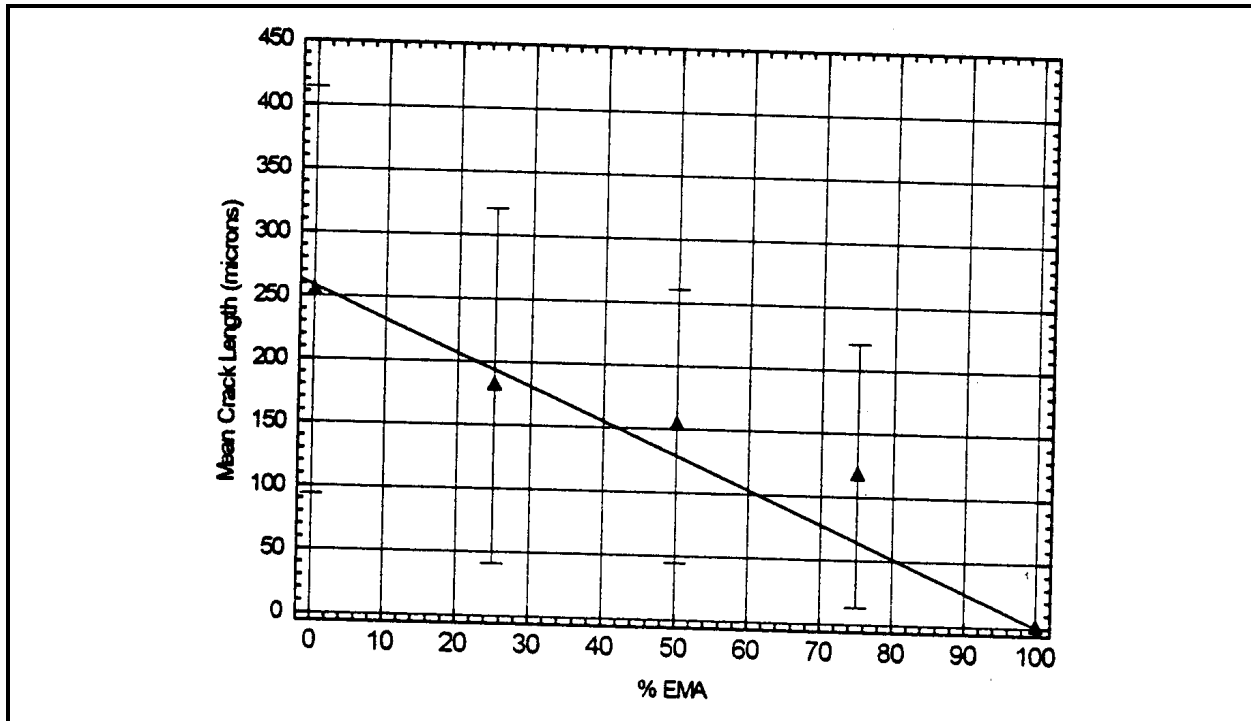


Figure 18. Average crack length for exposed coatings.

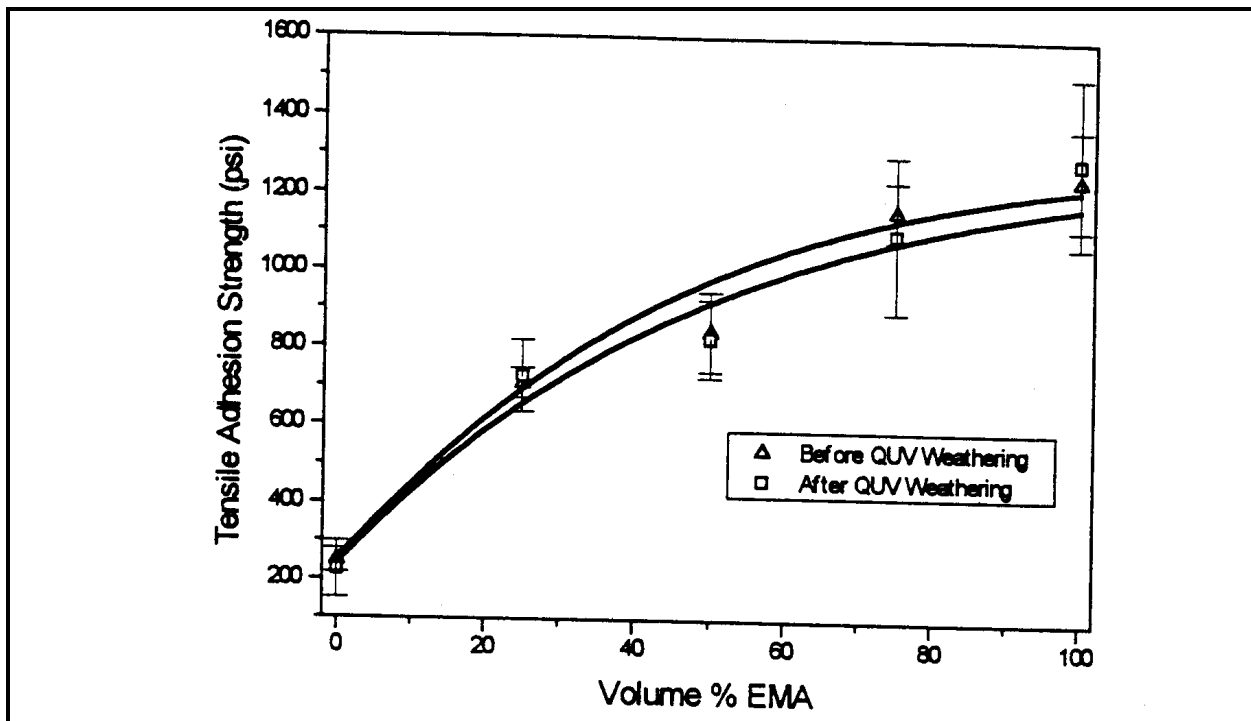


Figure 19. Tensile adhesion strengths for PCCP coating blends.

Table 5. Summary of spray-formed EMAA mechanical properties.

Coating	Secant Modulus at 5 percent strain (psi)	Yield Strength (psi)	Tensile Strength (psi)	Elongation to Break ( percent)	Toughness (lbs/inch)
PF113-pigment 104 °C	8426 ± 592	981 ± 38	1007 ± 43	78 ± 9	698 ± 106
PF113-pigment 160 °C	8081 ± 320	977 ± 23	1136 ± 23	268 ± 21	2789 ± 245
PF113-pigment 216 °C	8137 ± 460	969 ± 30	1115 ± 41	307 ± 42	3161 ± 502
PF113-clear 160 °C	7564 ± 207	970 ± 30	1178 ± 48	372 ± 43	3966 ± 565
PF113-clear 160 °C H <sub>2</sub> O quench	5020 ± 327	835 ± 73	1414 ± 113	683 ± 85	7350 ± 1168
PF111-clear 160 °C	8207 ± 456	1007 ± 21	1528 ± 28	407 ± 43	5192 ± 705
PF111-clear 216 °C	8266 ± 465	1074 ± 56	2338 ± 70	783 ± 33	12844 ± 895
PF111-clear 271 °C	6154± 237	936 ± 41	2028 ± 34	806 ± 19	11794 ± 352
PF111-pigment 216 °C	9278 ± 853	1114 ± 23	1727 ± 52	637 ± 38	8868 ± 588
PF111-clear 216 °C	5540 ± 214	985 ± 39	2437 ± 72	901 ± 29	14843 ± 611

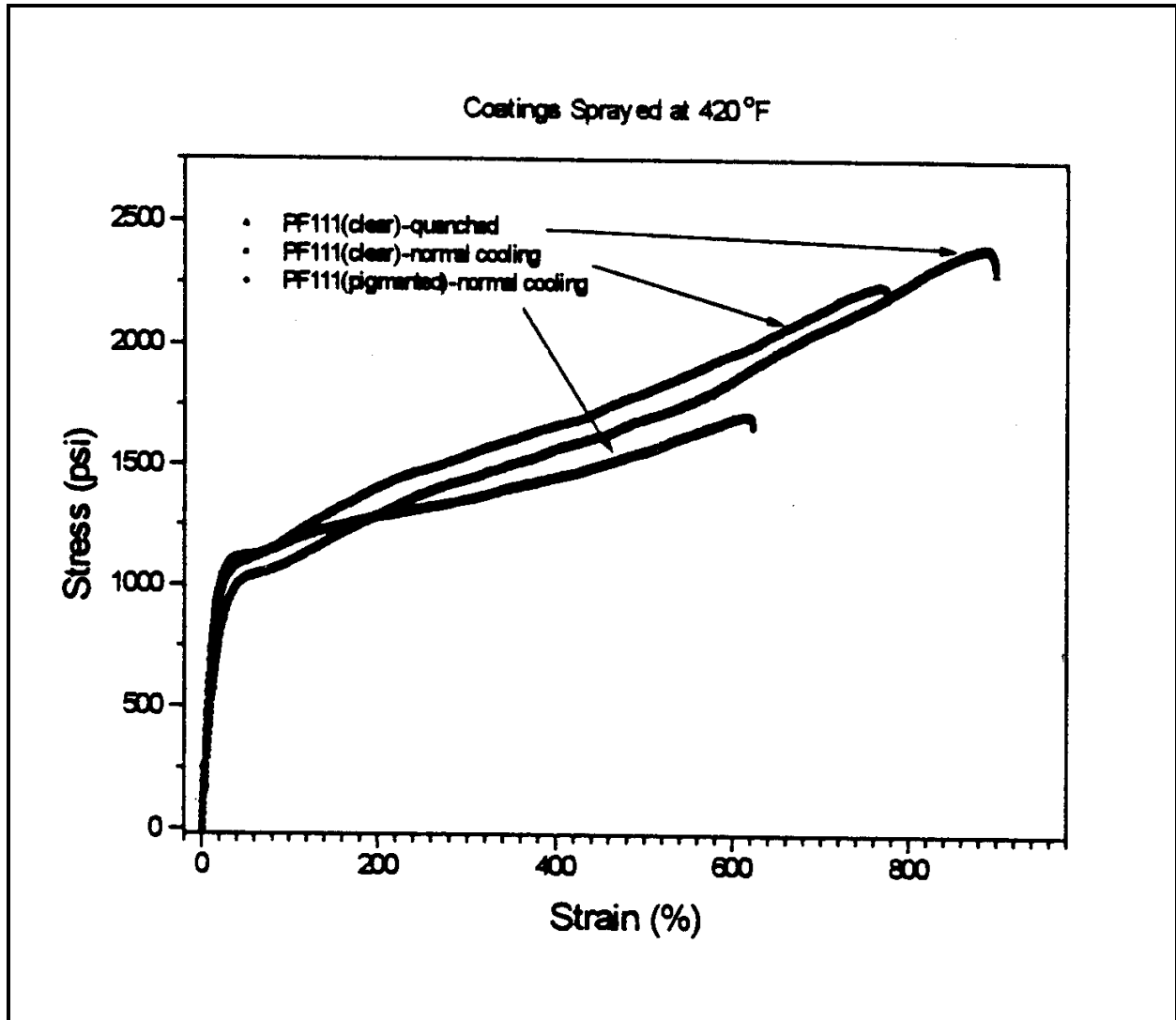


Figure 20. Stress-strain response of PF111 when pigmented, clear, and quenched.

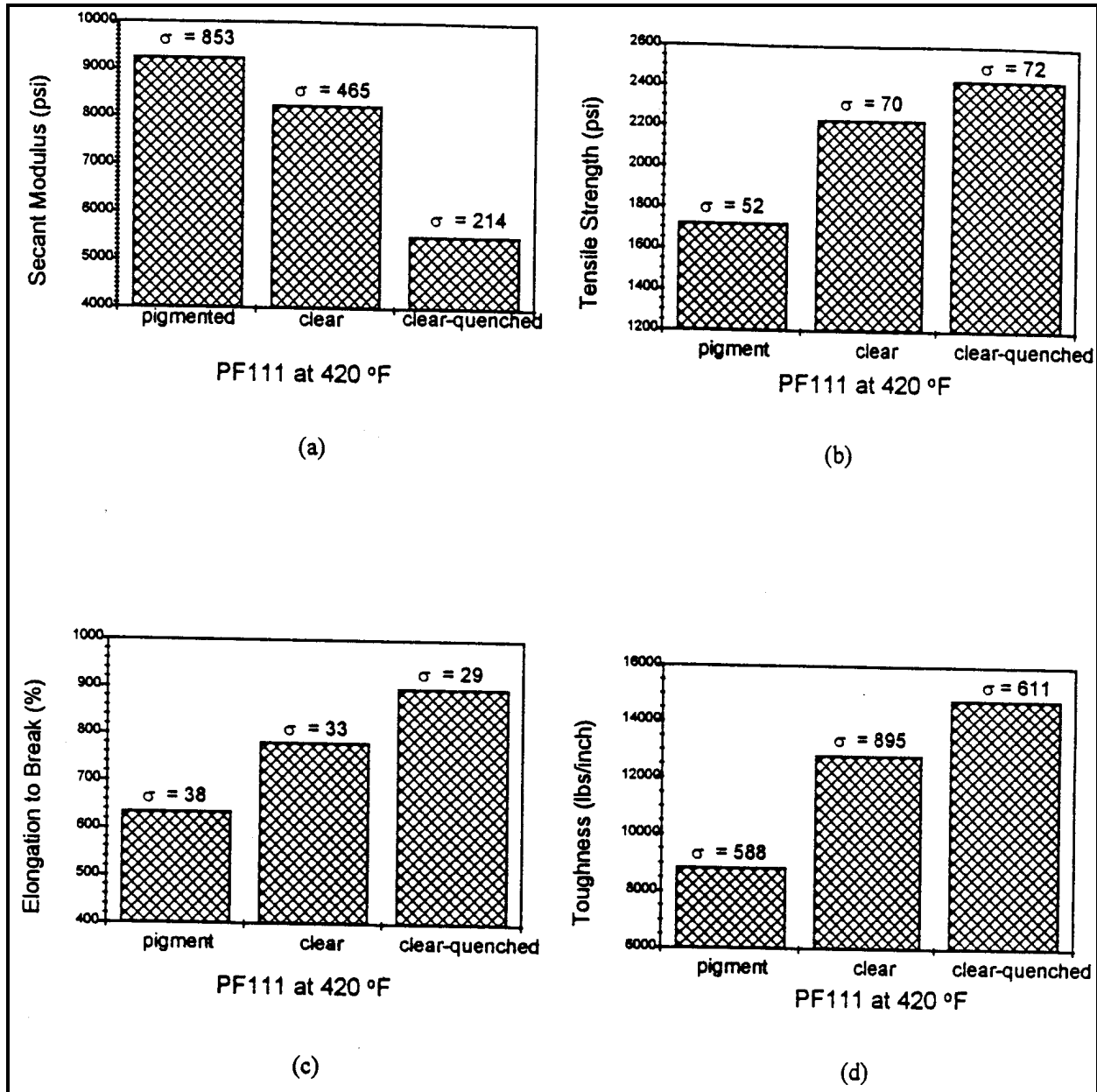


Figure 21. Selected mechanical properties for PF111: a) modulus, b) tensile, c) elongation to break, and d) toughness.

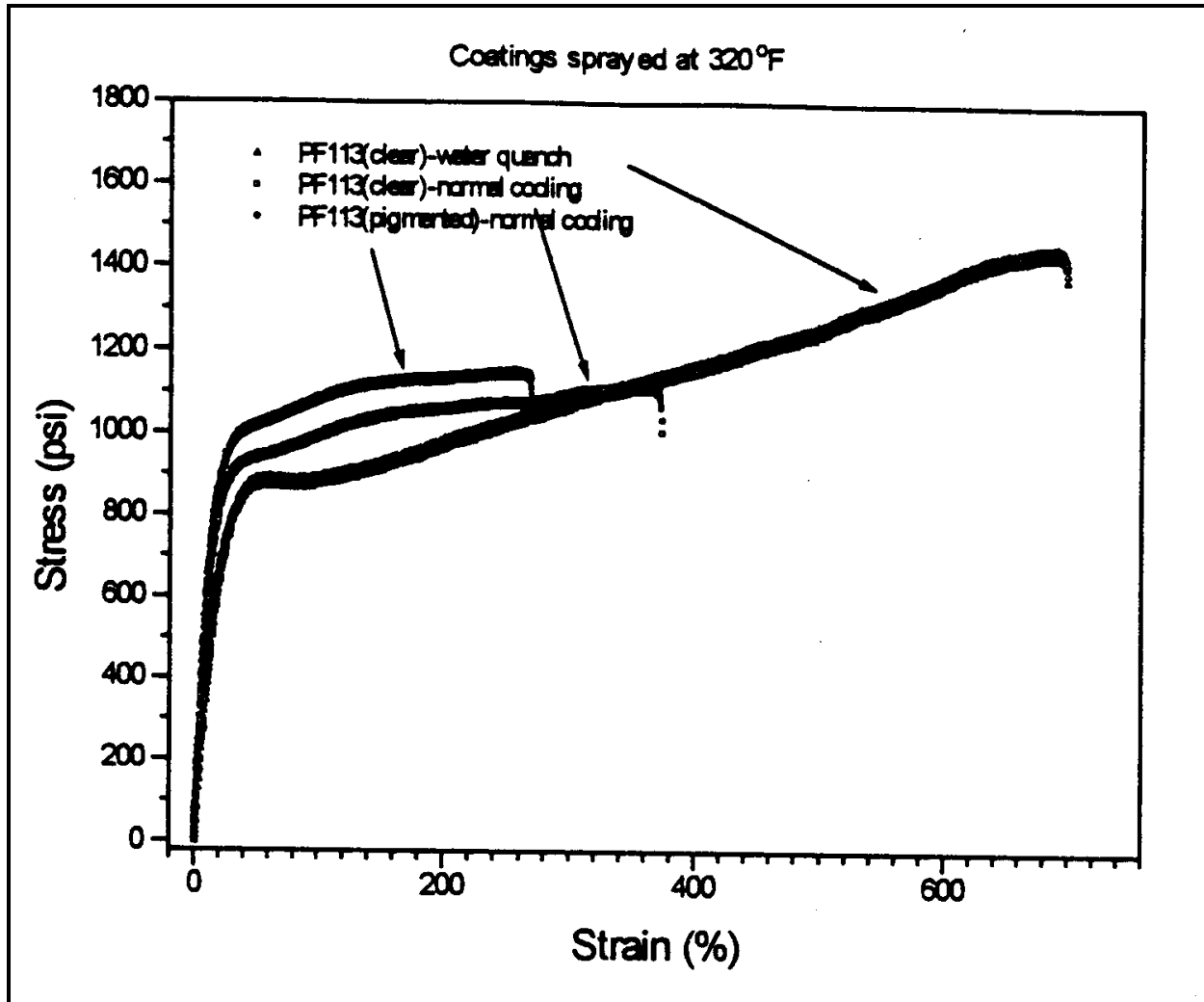


Figure 22. Stress-strain response for PF113 when pigmented, clear, and quenched.

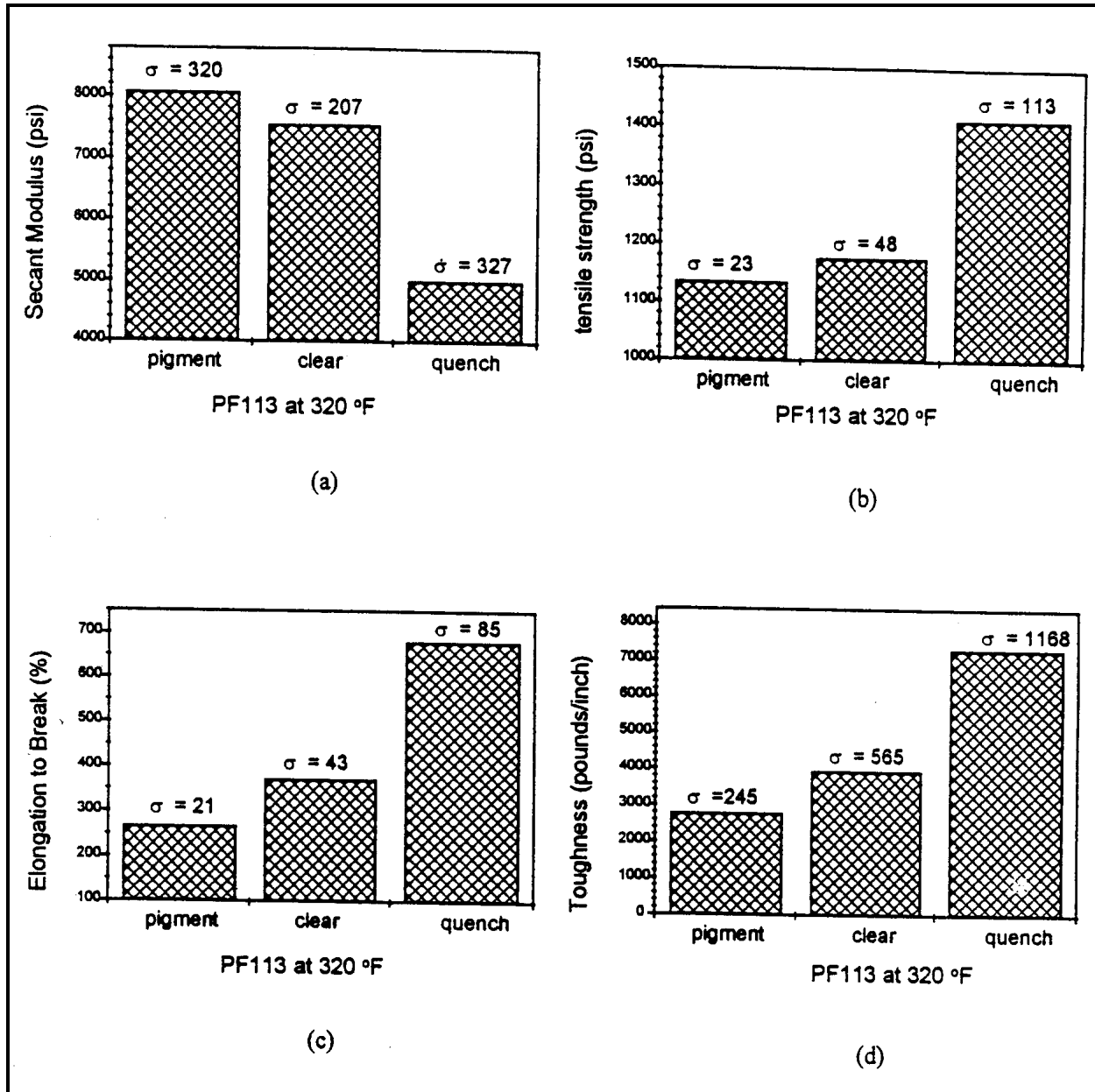


Figure 23. Selected mechanical properties for PF113: (a) modulus, (b) tensile, (c) elongation to break, and (d) toughness.

Table 6. Mechanical properties of melt-compounded PCCP with EMAA copolymer

Recycled Blend (PCCP:PF111)	Secant Modulus at 5 percent strain (psi)	Yield Strength (psi)	Tensile Strength (psi)	Elongation to Break ( percent)	Toughness (lb/inch)
10 percent PCCP	12283 ± 620	1279 ± 81	1296 ± 81	114 ± 18	1254 ± 277
20 percent PCCP	16259 ± 1355	1580 ± 83	1592 ± 98	62 ± 12	8777 ± 159
30 percent PCCP	19283 ± 998	1758 ± 76	1760 ± 80	31 ± 3	446 ± 60
40 percent PCCP	200992 ± 1091	1780 ± 49	1783 ± 50	25 ± 3	343 ± 54
50 percent PCCP	23986 ± 1225	1944 ± 74	1946 ± 46	19 ± 3	271 ± 35
60 percent PCCP	28644 ± 881	2176 ± 78	2179 ± 75	14 ± 1	219 ± 17
70 percent PCCP	32724 ± 1973	2269 ± 42	2270 ± 43	11 ± 0.5	160 ± 13
80 percent PCCP	34544 ± 868	2230 ± 199	2230 ± 200	8 ± 1	144 ± 28
90 percent PCCP	37926 ± 1593	2273 ± 55	2274 ± 56	7 ± 1	103 ± 14
100 percent PCCP	42723 ± 2857	2126 ± 197	2126 ± 197	5 ± 0.5	62 ± 11

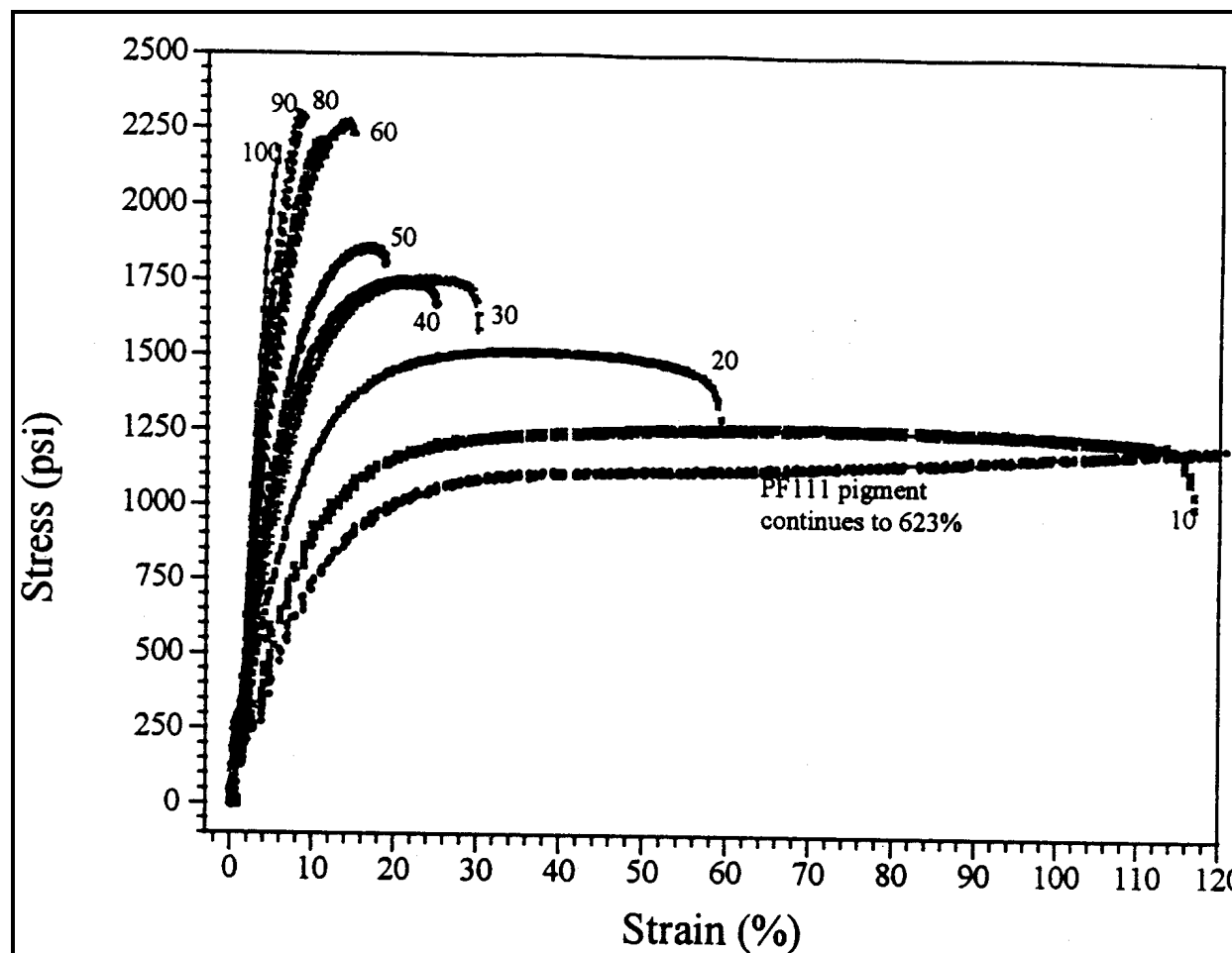
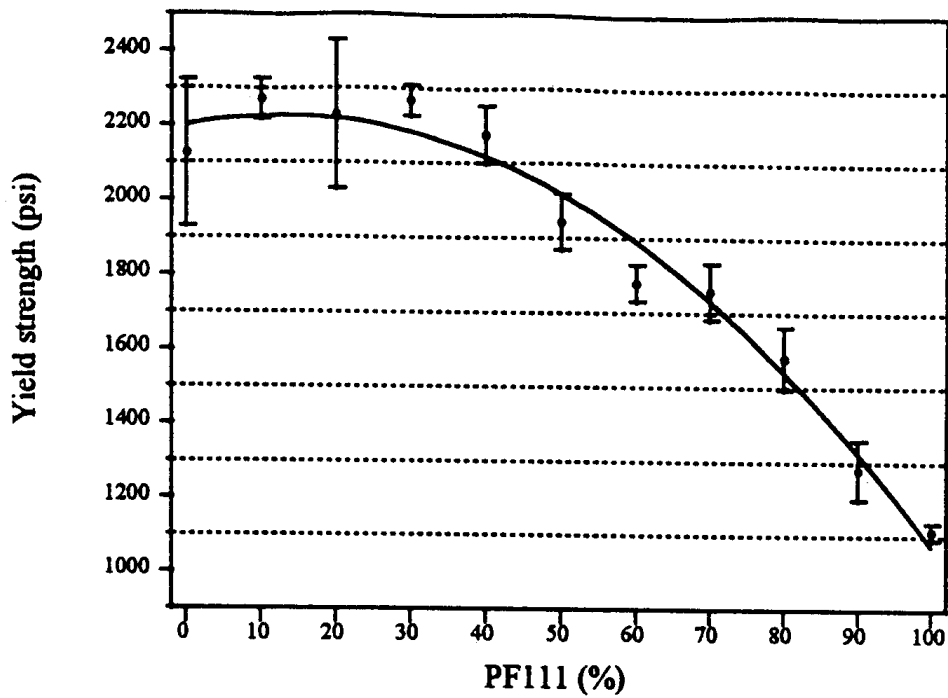
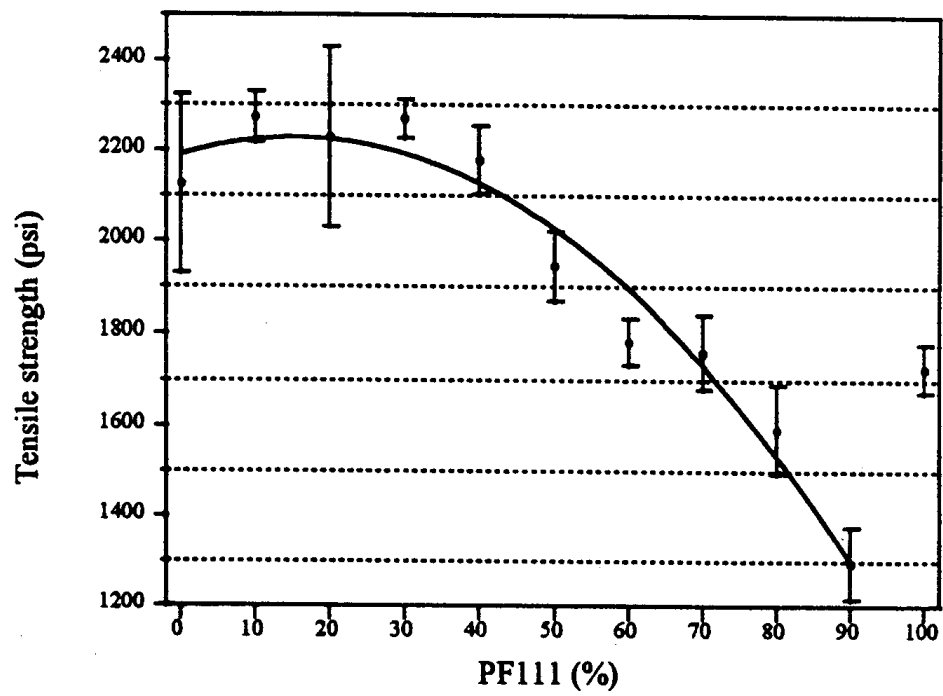


Figure 24. Stress-strain response for PCCP blends; volume percent PCCP noted on plot.

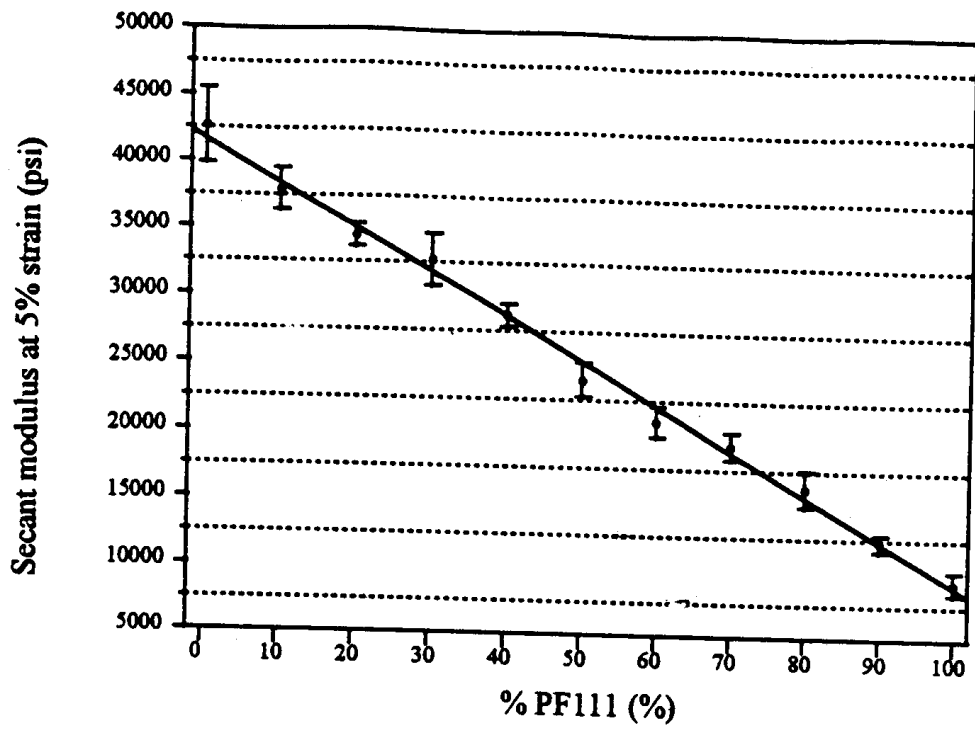


(a)

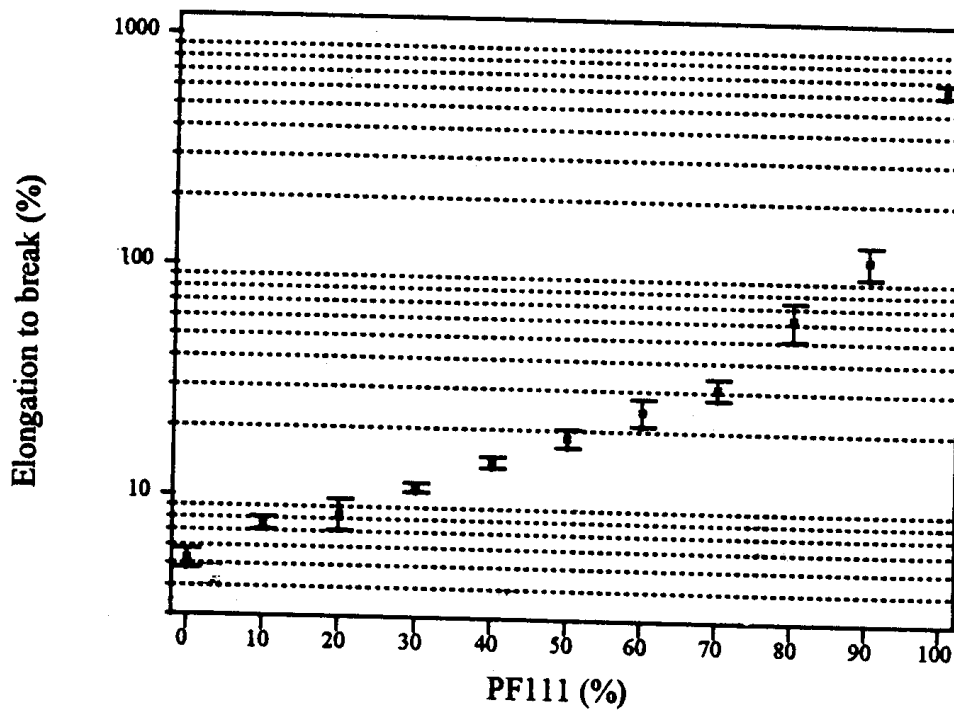


(b)

Figure 25. Mechanical properties of PCCP blends: (a) yield strength, (b) tensile strength, (c) secant modulus, and (d) elongation to break.



(c)



(d)

Figure 25. Continued.

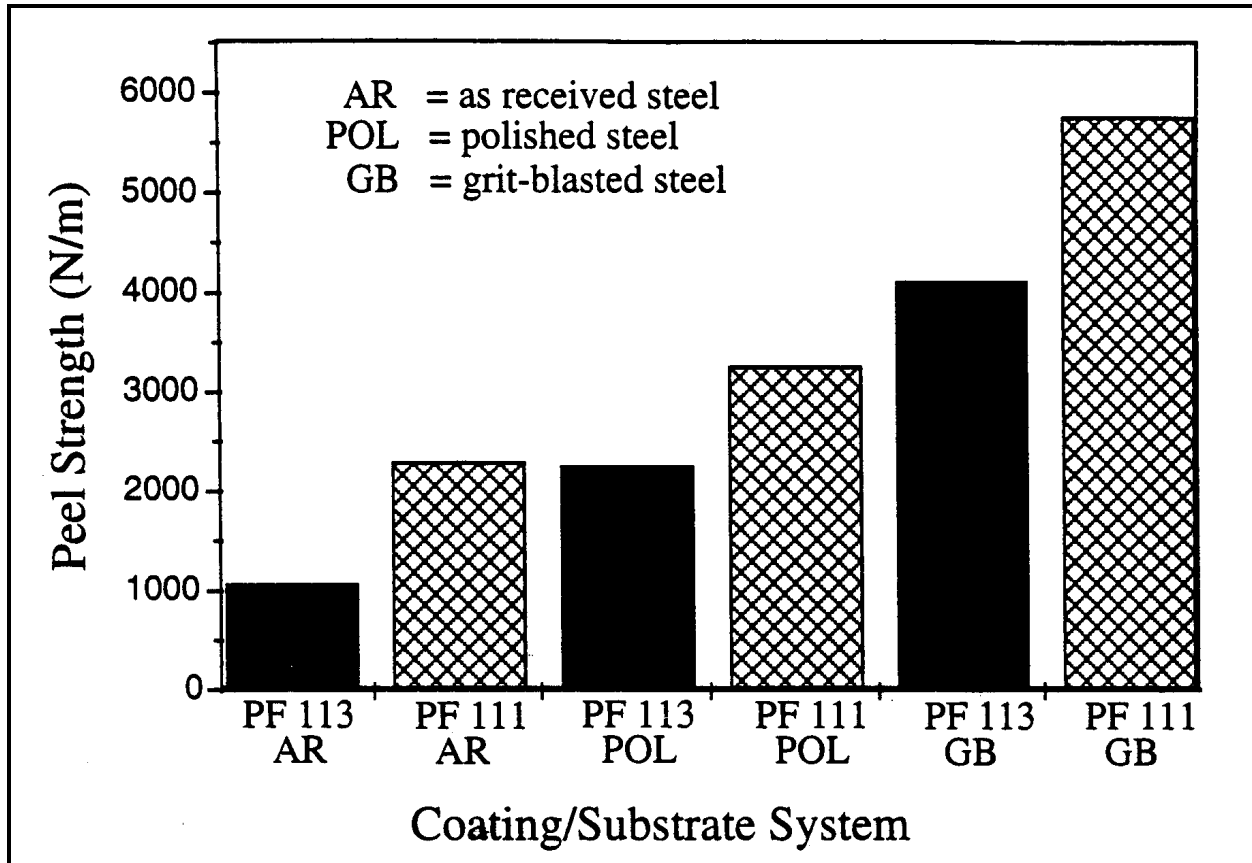


Figure 26. Summary of peel strength obtained for various steel surfaces.

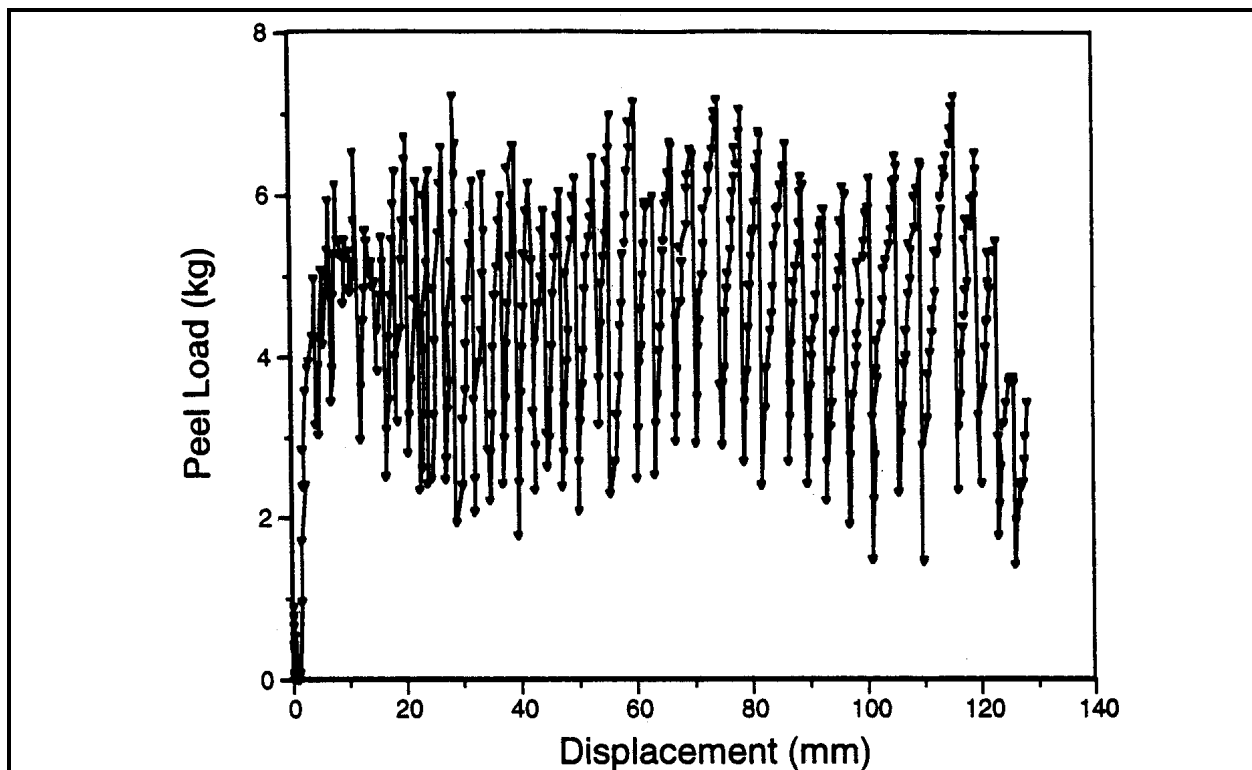


Figure 27. Load-displacement plot for PF111 on polished steel.

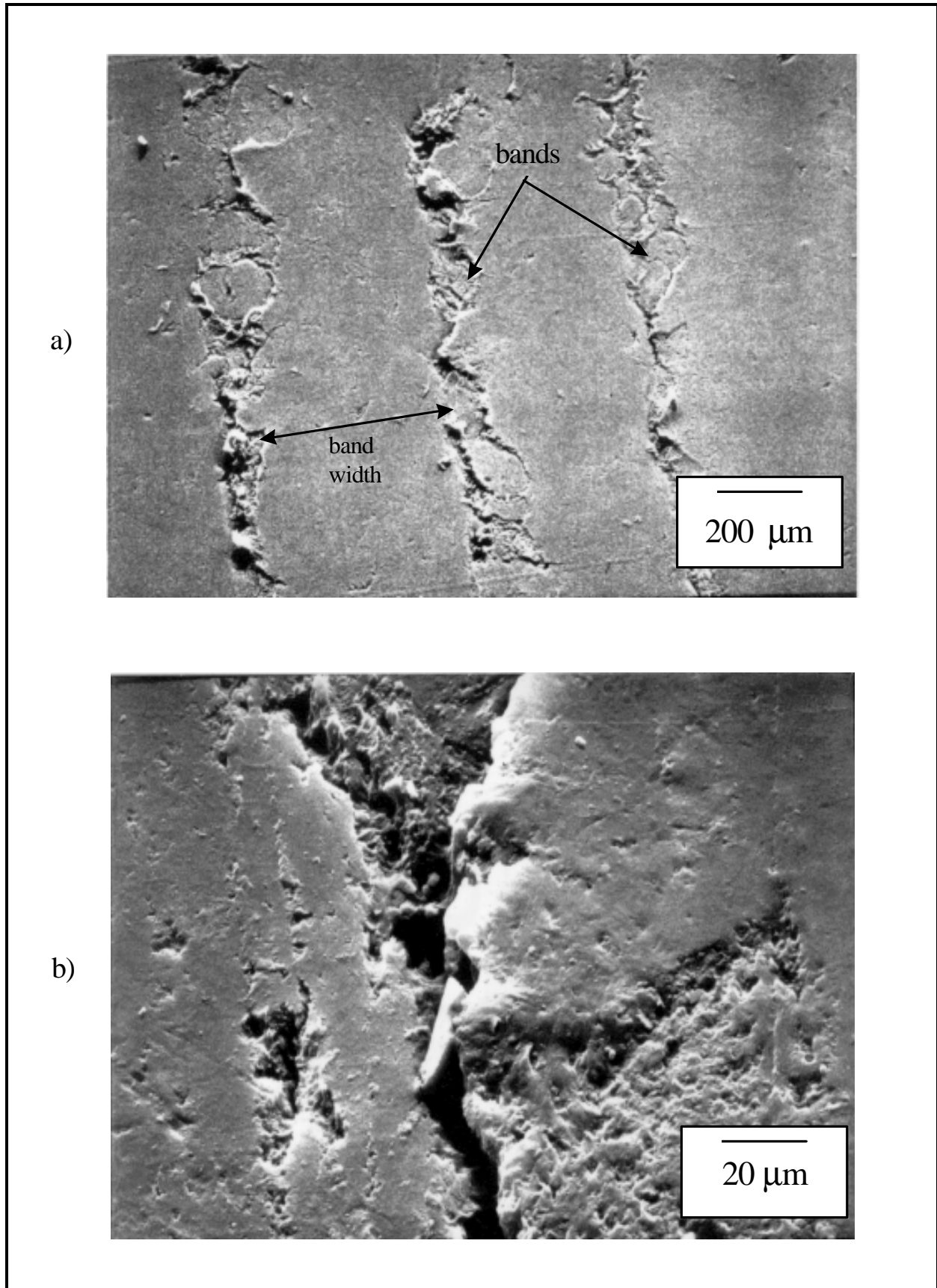


Figure 28. Polymer fracture surface from polished steel depicting bands at (a) low and (b) higher magnification.

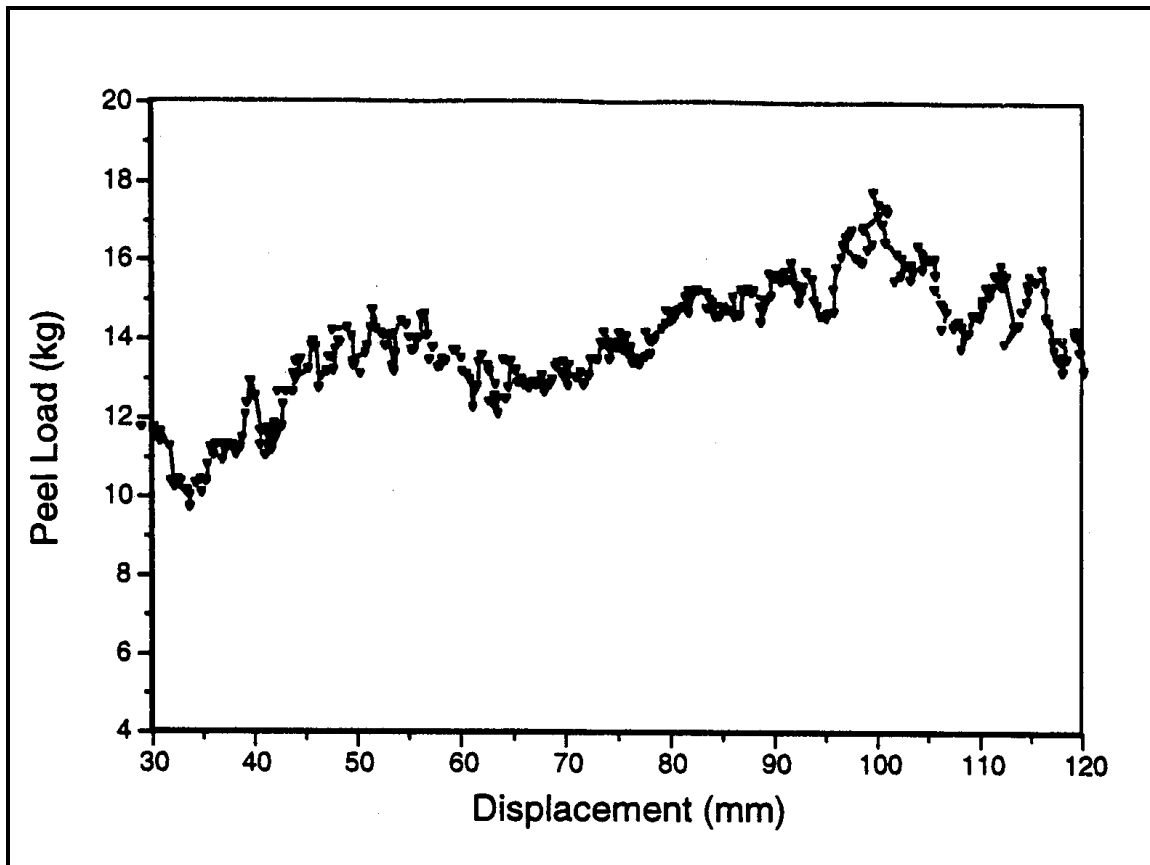


Figure 29. Load-displacement plot for PF111 on polished steel.

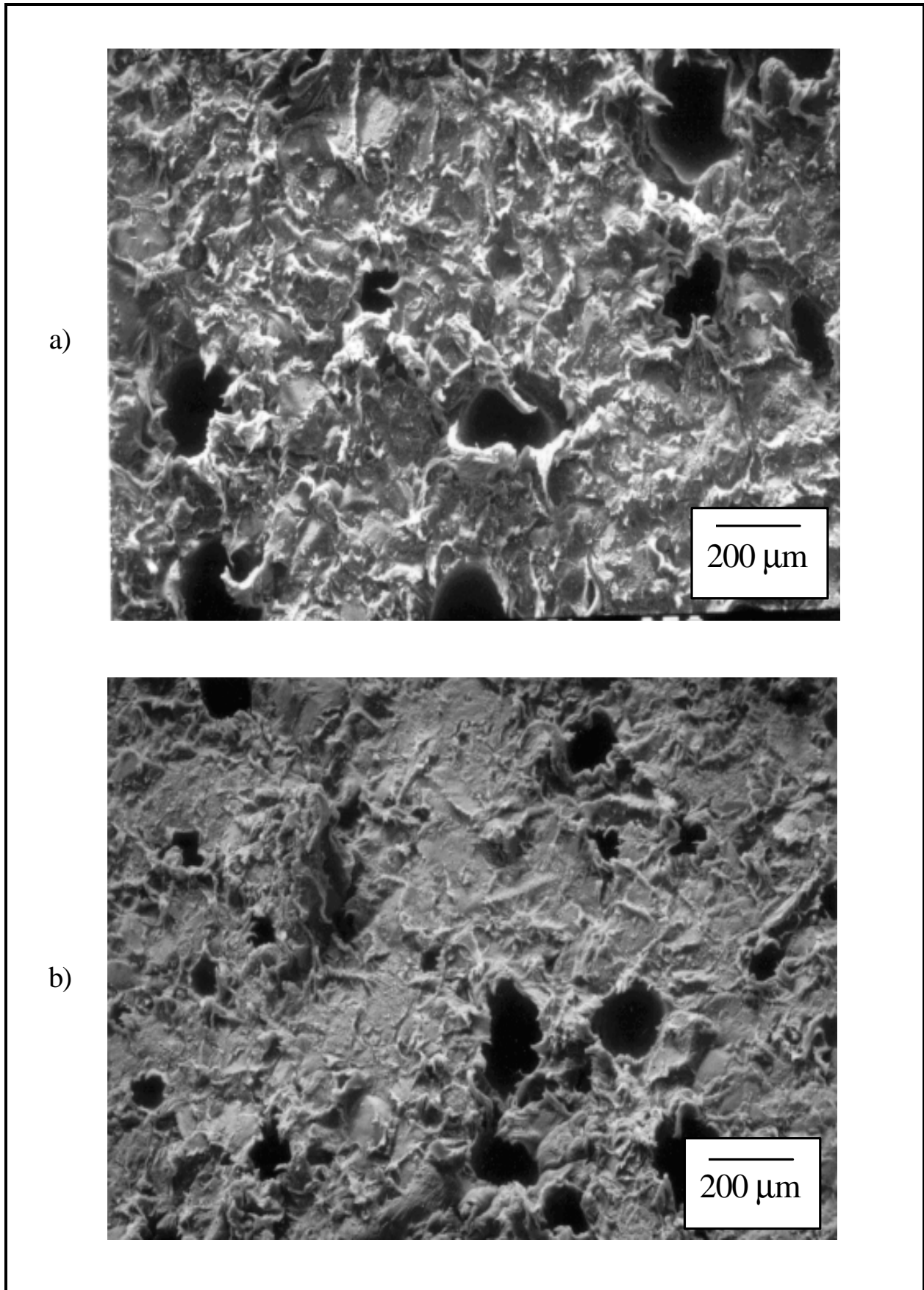


Figure 30. Peeling fracture surfaces from abrasive-blasted steel (a) PF111 and (b) PF113.

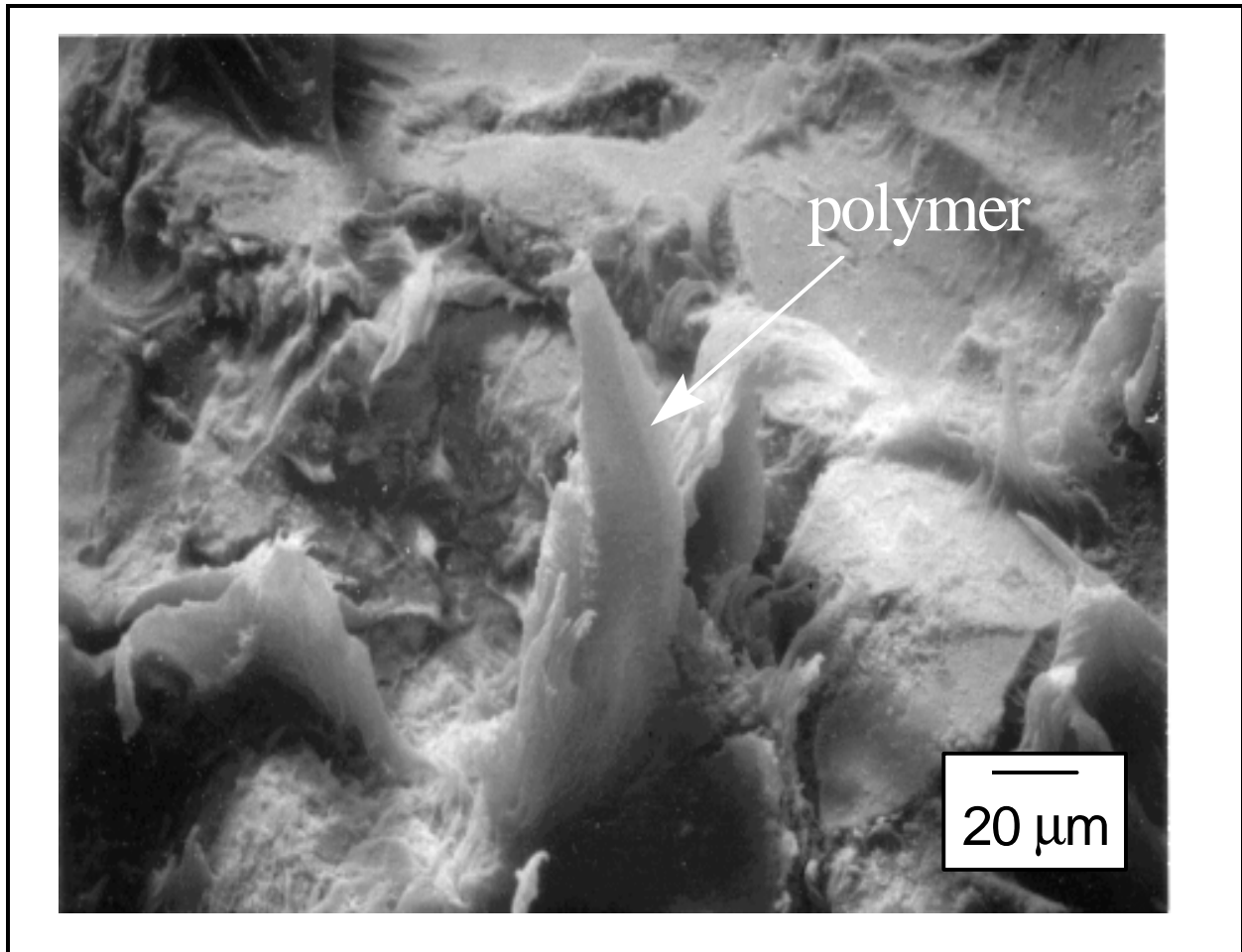


Figure 31. EMAA peeled from abrasive-blasted steel.

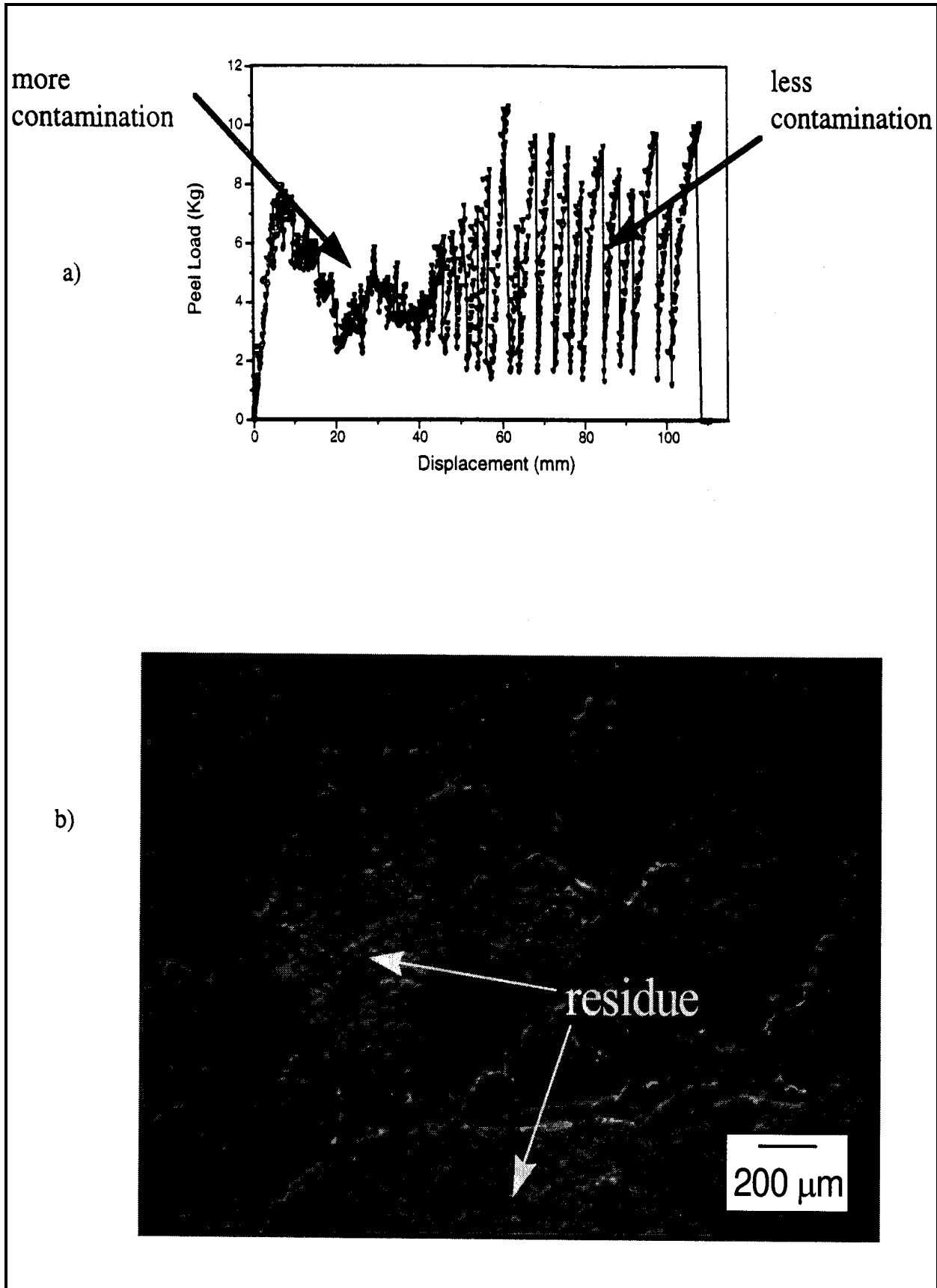


Figure 32. (a) Load displacement plot for as-received steel surface and (b) SEM micrograph of polymer coating surface.

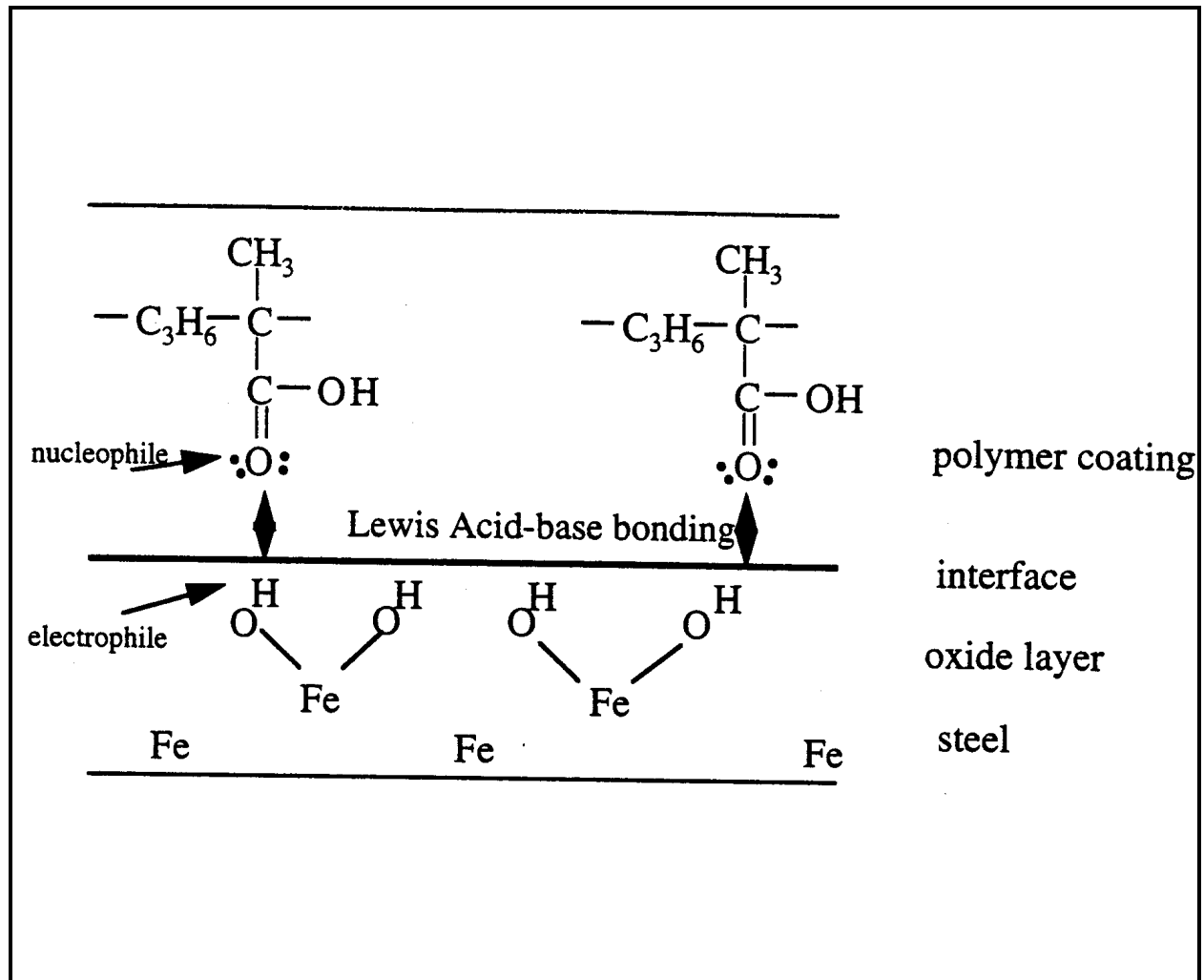


Figure 33. Proposed interfacial interactions between EMAA copolymer and steel oxide.

## 4 Field Application

Based upon preliminary results of this work, the Triborough Bridge and Tunnel Authority, New York, and SUNY Thermal Spray Laboratory personnel designated two bridge test sites. The first demonstration took place during the third week of August 1995 on Randall's Island Pier 4. Approximately 1200 ft<sup>2</sup> was abrasive-blasted to a 2-3 mil SP-6 profile. Both virgin ethylene methacrylic acid copolymer (PF111-grey) and a 3:1 blend of EMAA:PCCP were sprayed onto the designated areas.

The second demonstration was completed with the Triborough Bridge and Tunnel Authority during the third week of October 1995. Approximately 400 ft<sup>2</sup> was abrasive-blasted to a 2-3 mil SP-6 profile. Both virgin EMAA copolymer (PF111-grey) and a 3:1 blend of EMAA:PCCP were sprayed onto the designated areas. In addition, adjoining bridge sections were painted with a two-part alkyd system for comparison purposes.

In both test cases, the areas to be topcoated were preheated to 190 °F and a minimum of 20 mils of thermoplastic were applied (Figure 34). Inspection after 10 months of exposure found no signs of deterioration at either test site.

a)



b)



Figure 34. Field demonstration at the Triborough Bridge: (a) preheating the steel panel and (b) deposition of recycled polymer blend.

## 5 Cost Considerations

The addition of PCCP waste materials to virgin EMAA has the potential to reduce the materials cost of flame-sprayed polymer coating systems. Savings will be proportional to the volume of PCCP used. Using a 25 percent volume fraction of PCCP, net savings after processing costs is estimated at 15–20 percent below the cost for 100 percent virgin EMAA.

The total costs for field painting of steel structures are largely determined by the complexity of site setup, the degree of surface preparation required, and any requirements for highly skilled operators and specialized equipment. Materials comprise only a small portion of the total cost for surface preparation and thermal spray coating application. The percentage of total painting costs attributable to coating materials ranges from about 20 percent for a simple steel structure to less than 10 percent for structures that are intricate or difficult to access. Therefore, it can be seen that a 20 percent reduction in materials costs does not represent a significant savings in the total cost of a coating project, and this reduction is largely offset by additional costs of surface preparation and specialized equipment.

A number of low-VOC conventional paint systems are available that will adequately protect steel in atmospheric exposures. These can be applied with conventional paint spray equipment by workers with a moderate skill level. Many such coatings will tolerate an abrasive-blasted surface cleaned to a commercial or near-white grade at much lower cost than the white metal surface preparation grade recommended for flame-sprayed polymer coating systems.

## 6 Conclusions, Recommendations, and Commercialization

### Conclusions

A design of experiments approach was used to investigate the effects of material and application parameters on the melting and coalescence of a low molecular weight EMAA copolymer and high molecular weight PCCP. The substrate preheat temperature showed the largest effect on coating temperature. The powder injection rate had the largest effect on coating surface roughness and splat elongation ratio. The results of this study indicate that thermal sprayed EMAA/PCCP coatings should be applied only to surfaces that have been abrasive-blasted to the white metal grade.

Microstructures of the as-sprayed PCCP coatings (from dry-compounded powder) showed evidence of cracking. Accelerated weathering tests induced further cracking, photo-bleaching, and greater surface roughness.

The dry-compounded PCCP powder was blended with virgin EMAA in volumetric proportions of 25, 50, and 75 percent. Test results showed that the blending of EMAA with PCCP decreases the weathering-induced crack density and the average crack length as compared with unblended PCCP. No cracking was evident in the 100 percent EMAA coatings.

Blending the EMAA copolymer with PCCP also increased the adhesion to abrasive-blasted steel from 250 psi for 100 percent PCCP to 1100 psi for 25 percent PCCP. The 1250 hours of accelerated QUV weathering did not appreciably affect coating adhesion. Melt-compounded PCCP has greater strength and a higher modulus in comparison to virgin EMAA. However, coating toughness can be improved by incorporating EMAA into the feedstock.

In summary, it is concluded that the incorporation of PCCP into virgin EMAA material is associated with some loss of performance. Cost savings resulting from the blending 25 percent PCCP with 75 percent virgin EMAA are insignificant

compared to the total cost of a recoating job. Therefore, it is expected that the use of PCCP/EMAA will have only a very limited commercial usefulness.

## Recommendations

The use of PCCP/EMAA is not recommended as a protective coating for steel structures.

## Commercialization and Technology Transfer

A draft Civil Works Guide Specification (CWGS) was to have been prepared for this technology upon conclusion of the work. However, the unremarkable performance of PCCP/EMAA blends in this investigation indicates that the preparation of such a specification would be highly premature.

The State University of New York continues to monitor coating performance at the two field demonstration sites and conduct related research. If the SUNY researchers are able to overcome the technical problems shown in this study, they will initiate work with the Steel Structures Painting Council and other standards organizations to develop materials standards and application guidance.

The State University of New York maintains responsibility for the commercialization of the polymer coatings. SUNY has undertaken an extensive technology transfer program to promote commercialization of this technology. To date this program has included the activities noted below.

### ***Patent Disclosure***

J. Brogan, C.C. Berndt, R. Lampo, K.A. Gross, S. Sampath, and H. Herman, *Thermal Spraying of Recycled and Post-Consumer Commingled Polymer Material*, S-7088, disclosed 17 November 1994.

### ***Invited Presentations***

1. *A Comprehensive Approach Towards the Maintenance of Infrastructural Steel*, Northwestern University Infrastructure Technology Institute, Absecon, NJ, 1–3 November 1995.
2. *The Role of Academia: Strategic Partnerships for Advancing Thermal Spray Technology*, National Thermal Spray Conference (NTSC '95), Thermal Spray Society, 10 September 1995.

3. Presentation to the Welding Research Council Subcommittee on Hardfacing and Wear, 21 April 1995.

### **Conferences**

1. 4th World Congress on Coating Systems for Bridges and Steel Structures, 1-3 February, 1995, St. Louis, MO (two presentations)
2. National Association of Corrosion Engineers, 27-31 March, 1995, Orlando, FL (one paper presented)
3. American Welding Society, 3-7 April, 1995, Cleveland, OH (one paper presented)
4. National Association of Corrosion Engineers, 23-28 March, 1996, Denver, CO
5. 1996 VIII International Congress on Experimental and Applied Mechanics, June 10-13, Nashville, TN (one paper presented)
6. ASM International, 5th National Thermal Spray Conference, May 1994, Boston, MA (eight papers)
7. ASM International, 6th National Thermal Spray Conference, 11-15 September 1995, Houston, TX (six papers)
8. Civil Engineering Research Foundation (CERF) Meeting on Infrastructure, 1-3 April 1995, Washington, DC.

### **Selected Publications**

1. S.H. Leigh and C.C. Berndt, "A Test for Coating Adhesion on Flat Substrates— A technical note," *JTST* 3[2] (1994), pp 184-190.
2. T. Sugama, R. Kawase, C.C. Berndt, and H. Herman, "An Evaluation of Methacrylic Acid-modified Polyethylene Coatings Applied by Flame-spray Technology," *Progress in Organic Coatings*, 25[2] (1995), pp 205-216.
3. J.A. Brogan and C.C. Berndt, "The Coalescence of Combustion Sprayed Ethylene-Methacrylic Acid Copolymer," accepted for *J.Mater. Sci.*, April 1996.
4. J.A. Brogan, C.C. Berndt, W.C. Smith, R.V. Gansert, S. Raghu, S. Sampath, and H. Herman, "Real-time Imaging of the Plasma Spray Process—work in Progress," *JTST*, 4[4] (1995), pp 374-376.
5. J.A. Brogan, K.A. Gross, Z. Chen, H. Herman, and C.C. Berndt, "Investigation of Combustion Sprayed Hydroxyapatite/polymer Composite Coatings," pp 159-164 in *1994 Thermal Spray Industrial Applications*, ed., C.C. Berndt and S. Sampath (ASM International, Materials Park, OH, 1994).
6. J.A. Brogan, R. Lampo, and C.C. Berndt, "Thermal Spraying of Polymers," *Proc. 4th World Congress on Coating Systems for Bridges and Steel Structures*, 1-3 February, 1995, St. Louis, MO, pp 200-212.

7. J.A. Brogan, J. Margolies, S. Sampath, H. Herman, C.C. Berndt, and S. Drozd, "Adhesion of Combustion-Sprayed Polymer Coatings," pp 521-526 in *1995 Advances in Thermal Spray Science and Technology*, ed. C.C. Berndt and S. Sampath (ASM International, Materials Park, OH, 1995).
8. C.C. Berndt, M.L. Allan, H. Herman, J. Brogan, R. Benary, R. Zatorski, and M. Leote, "Thermal Spray Technologies for Infrastructure Repair and Maintenance," extended abstract for *Proc. of the VIII International Congress on Experimental Mechanics*, Pub. SEM, CT-USA, 1996.
9. *World Wide Web Home Page*. An informational home page is located at <http://dol1.eng.sunysb.edu/berndt.html>.

## References

1. T. Katauskas, "DOT Coats Rusting Bridges with Layers of Problems," Research and Development, May, (1990) pp 42-48.
2. T. Race, V. Hock and A. Beitelman, "Performance of Selected Metallized Coatings and Sealers on Lock and Dam Facilities," J. Protective Coatings & Linings, 6 [1], Jan. 1989, p 37-44.
3. J.A. Apostolos, D.M. Parks, and R.A. Carello, "Cathodic Protection using Metallized Zinc," Materials Performance, 26 [12], (1987) p 22-28.
4. R.H. Unger, "Thermal Spraying of Bridges," Thermal Spray: Advances in Coating Technology, Ed. by D. Houck, ASM, (1988) p 399-406.
5. G.K. Sweet, "Applying Thermoplastic/Thermoset Powder with a Modified Plasma System," Thermal Spray Coatings: Research Design and Applications, Ed. by C.C. Berndt and T.F. Bernecki, ASM, (1993) p 381-384.
6. P. J. Loustaunau and D. Horton, "EMAA Thermoplastic Powder Coatings in Shop and Field Applications," Materials Performance, July (1994) p 32-35.
7. J. Maty, "Reg-Neg Plan Likened to L.A. Rules," American Paint and Coatings Journal, 78 [8], 1993.
8. A. Rogerson, "CALTRANS Tests Powder Coatings in the Field," J. Protective Coatings and Linings, 11 [8] (1994) p 25-32.
9. T. Race, "Evaluation of Flame-Sprayed Polymer Coatings for Civil Works Navigation Structures," USACERL Technical Report FM-94/07, April 1994.
10. T.W. Glass and J.A. dePay, "Protective Thermoplastic Powder Coating Specifically Designed Adhesive Polymers," Thermal Spray Coatings: Properties, Processes and Applications, Edited by T.F. Bernecki, ASM, (1991) p 345-351.
11. J.A. Brogan, K.A. Gross, Z.Chen, C.C. Berndt, H. Herman, "Investigation of Combustion Sprayed Hydroxyapatite/Polymer Composite Coatings," Thermal Spray Industrial Applications, Edited by C.C. Berndt and S. Sampath, ASM, (1994) p 159-163.
12. Y. Bao and D.T. Gawne, "Plasma Spraying of Glass-Polyamide Composite Coating," Thermal Spray Coatings: Research Design and Applications, Edited by C.C. Berndt and T.F. Bernecki, ASM, (1993) p 417-422.
13. J.A. Brogan and S. Reddy - 1994 Dupont Plunket Student Award.
14. J. Reimer, "Method and Apparatus for Spray Coating," US Patent 4,632,309 Dec. 30, 1986, 11p.

15. J. Agapakis and T. Hoffman, "Real-Time Imaging for Thermal Spray Process Development and Control," *JTST*, 1 [1] (1992) p 19-25.
16. J.A. Brogan and C.C. Berndt "The Coalescence of Combustion-Sprayed Ethylene Methacrylic Acid Copolymer," accepted for publication in *J.Mat.Sci*.
17. E.P. Box, W.G. Hunter, and J.S. Hunter, *Statistics for Experimenters*, John Wiley and Sons, New York, 1978.
18. J. Kolarik, "Evaluation of the Extent of Interfacial Debonding in Polymer Blends," *Polymer*, 37 [6] (1996) p 887-891.
19. Z. Horak, V. Fort, D.Hlavata, F. Lednický, and F. Vecerka, "Compatibilization of High Impact Polystyrene/Polypropylene Blends," *Polymer*, 37 [1] (1996) p 65-73.
20. D.J. Ihm and J. White, "Interfacial Tension of Polyethylene/Polyethylene Terephthalate with Various Compatibilizing Agents," *J. Applied Polymer Science*, 60 (1996) p 1-7.
21. K.S. Kim and N. Aravas, "Elastoplastic Analysis of the Peel Test," *Int. J. Solids Structures*, 24 [4] (1988) p 417-435.
22. A.N. Gent, and G.R. Hamed, "Peel Mechanics for an Elastic-Plastic Adherend," *J. Appl. Polym. Sci.*, 21, (1977) p 2817-2831.
23. M.Sexsmith and T. Troczynski, "Peel Adhesion Test for Thermal Spray Coating," *JTST*, 3 [4] (1994) p 404-411.
24. J.A. Brogan, J. Margolies, S. Drozd, S. Sampath, H. Herman, and C.C. Berndt, "Adhesion of Combustion Sprayed Polymer Coatings," 1995 *Advances in Thermal Spray Science and Technology*, Ed. by S. Sampath and C.C. Berndt, ASM, (1995), p 521-526.
25. F.M. Fowkes, "Role of Acid-Base Interfacial Bonding in Adhesion," *J. Adhesion Sci, Tech.*, 1 [1] (1987) p 7-27.
26. F.M. Fowkes, "Quantitative Characterization of the Acid-Base Properties of Solvents, Polymers, and Inorganic Surfaces," *J. Adhesion Sci. Techn.*, 4 [8] (1990) p 669-691.
27. ASTM C 633-79, *Test Method for Adhesion or Cohesive Strength of Flame-Sprayed Coatings* (ASTM International, Philadelphia, PA, 1993).
28. ASTM D 638-94b, *Test Method for Tensile Properties of Plastics* (ASTM International, Philadelphia, PA, 1994).
29. ASTM D 3167-93, *Test Method for Floating Roller Peel Resistance of Adhesives* (ASTM International, Philadelphia, PA, 1993).
30. ASTM G 53-94, *Practice for Operating Light- and Water-Exposure Apparatus (Fluorescent UV-Condensation Type) for Exposure of Nonmetallic Materials* (ASTM International, Philadelphia, PA, 1994).

## Appendix: Equipment and Instrumentation Vendors

Plastic Flamecoat Systems 1613-T Hwy 3 League City, TX 77573 (713)332-8180	Applied Test Systems, Inc. PO Box 1529 Butler, PA 16003 (412)283-1212
Tinius Olsen Testing Machine Co. Easton Road Willow Grove, PA 19090 (215)675-7100	Stat-Ease, Inc. 2021-T E. Hennepin Ave, Suite 191 Minneapolis, MN 55413 (612)378-2152
Control Vision, Inc. PO Box 51505 Idaho Falls, ID 83405 (208)523-5506	Buehler Ltd. 41 Waukegan Road Lake Bluff, IL 60044 (800)283-4537
Unitrol, Inc. 170-T Wilbur Place Bohemia, NY 11716 (516)589-6666	Obex, Inc. PO Box 1253 Stamford, CT 06904 (203)975-9094
Perkin-Elmer Corp. Metco Division PO Box 1006 Westbury, NY 11590 (516)334-1300	

**USACERL DISTRIBUTION**

## Chief of Engineers

ATTN: CEHEC-IM-LH (2)

ATTN: CEHEC-IM-LP (2)

ATTN: CECW

ATTN: CECW-OM

ATTN: CECW-P

ATTN: CECW-PR

ATTN: CERD-L

ATTN: CERD-C (2)

## CECPW 22310-3862

ATTN: CECPW-E

ATTN: CECPW-FT

ATTN: CECPW-ZC

## US Army Engr District

ATTN: Library (40)

## US Army Engr Division

ATTN: Library (11)

## Defense Tech Info Center 22304

ATTN: DTIC-O (2)

67  
12/98